AD-A174 893 NUCLEAR HARDNESS SIMULATION AND ANALYSIS OF COMPOSITE AIRCRAFT STRUCTURES (U) GENERAL RESEARCH CORP SANTA BARBARA CA W F ADLER 31 DEC 85 GRC-CR-85-1408 1/1

UNCLASSIFIED DNA-TR-86-132-V2 DNA001-82-C-0245 F/G 11/4 NL

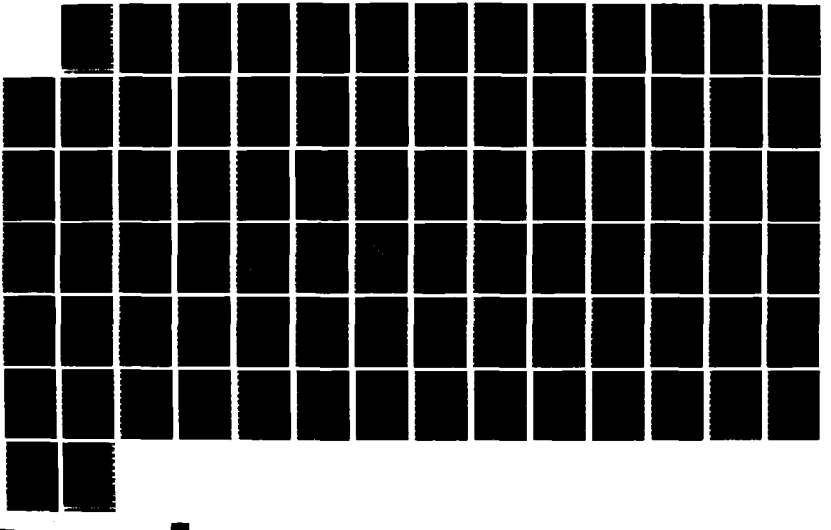

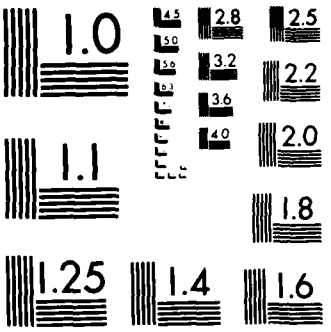

(12)

DNA-TR-86-132-V2

NUCLEAR HARDNESS SIMULATION AND ANALYSIS OF COMPOSITE AIRCRAFT STRUCTURES

Volume II—Dust Erosion Assessment

W. F. Adler
General Research Corporation
Santa Barbara Division
P. O. Box 6770
Santa Barbara, CA 93160-6770

31 December 1985

Technical Report

CONTRACT No. DNA 001-82-C-0245

THIS WORK WAS SPONSORED BY THE DEFENSE NUCLEAR AGENCY
UNDER RDT&E RMSS CODE B342083466 N99QAXAJ00029 H2590D.

Prepared for
Director
DEFENSE NUCLEAR AGENCY
Washington, DC 20305-1000

DISTRIBUTION LIST UPDATE

This mailer is provided to enable DNA to maintain current distribution lists for reports. We would appreciate your providing the requested information.

☐ Add the individual listed to your distribution list.

☐ Delete the cited organization/individual.

☐ Change of address.

NAME: _____

ORGANIZATION: _____

OLD ADDRESS	CURRENT ADDRESS
_____	_____
_____	_____
_____	_____

TELEPHONE NUMBER: ( ) _____

SUBJECT AREA(s) OF INTEREST:

_____	_____
_____	_____
_____	_____

DNA OR OTHER GOVERNMENT CONTRACT NUMBER: _____

CERTIFICATION OF NEED-TO-KNOW BY GOVERNMENT SPONSOR (if other than DNA):

SPONSORING ORGANIZATION: _____

CONTRACTING OFFICER OR REPRESENTATIVE: _____

SIGNATURE: _____

Director
Defense Nuclear Agency
ATTN: STTI
Washington, DC 20305-1000

Director
Defense Nuclear Agency
ATTN: STTI
Washington, DC 20305-1000

UNCLASSIFIED
SECURITY CLASSIFICATION OF THIS PAGE

AD-A174 893

REPORT DOCUMENTATION PAGE

1a. REPORT SECURITY CLASSIFICATION UNCLASSIFIED	1b. RESTRICTIVE MARKINGS
2a. SECURITY CLASSIFICATION AUTHORITY N/A since UNCLASSIFIED	3. DISTRIBUTION/AVAILABILITY OF REPORT Approved for public release; distribution is unlimited.
2b. DECLASSIFICATION/DOWNGRADING SCHEDULE N/A since UNCLASSIFIED	
4. PERFORMING ORGANIZATION REPORT NUMBER(S) CR-85-1408	5. MONITORING ORGANIZATION REPORT NUMBER(S) DNA-TR-86-132-V2
6a. NAME OF PERFORMING ORGANIZATION General Research Corporation Santa Barbara Division 6b. OFFICE SYMBOL (If applicable)	7a. NAME OF MONITORING ORGANIZATION Director Defense Nuclear Agency
6c. ADDRESS (City, State, and ZIP Code) P. O. Box 6770 Santa Barbara, CA 93160-6770	7b. ADDRESS (City, State, and ZIP Code) Washington, DC 20305-1000
8a. NAME OF FUNDING/SPONSORING ORGANIZATION 8b. OFFICE SYMBOL (If applicable)	9. PROCUREMENT INSTRUMENT IDENTIFICATION NUMBER DNA 001-82-C-0245
8c. ADDRESS (City, State, and ZIP Code)	10. SOURCE OF FUNDING NUMBERS PROGRAM ELEMENT NO. 62715H; PROJECT NO. N99QAXA; TASK NO. J; WORK UNIT ACCESSION NO. DH006197

11. TITLE (Include Security Classification)
NUCLEAR HARDNESS SIMULATION AND ANALYSIS OF COMPOSITE AIRCRAFT STRUCTURES
Volume II—Dust Erosion Assessment

12. PERSONAL AUTHOR(S)
Adler, W. F.

13a. TYPE OF REPORT	13b. TIME COVERED	14. DATE OF REPORT (Year, Month, Day)	15. PAGE COUNT
Technical	FROM 820630 TO 841130	851231	84

16. SUPPLEMENTARY NOTATION
This work was sponsored by the Defense Nuclear Agency under RDT&E RMSS Code B342083466 N99QAXAJ00029 H2590D.

17. COSATI CODES			18. SUBJECT TERMS (Continue on reverse if necessary and identify by block number)
FIELD	GROUP	SUB-GROUP	Dust Erosion, Composite Materials, Rain Erosion, Mass Loss, Erosion Modeling
11	4		
13	13		

19. ABSTRACT (Continue on reverse if necessary and identify by block number)

This second volume of a two-volume report assesses the state of dust erosion data for composite materials. A survey of the solid particle erosion literature revealed that some experimental data is available for polymeric materials and fiber-reinforced, non-metallic composites. Although not directly applicable to the specific compositions currently of interest, the available data is used to provide initial insights into the magnitude of the erosion problems which may exist for advanced composite materials on aircraft flying through nuclear-generated dust. Using published erosion data, the possibility exists for a significant amount of material removal to occur. Additional investigations are suggested to provide a more relevant estimate of the magnitude of the dust erosion problem. The report also discusses available test facilities and their capabilities and presents an extensive bibliography of relevant literature.

20. DISTRIBUTION/AVAILABILITY OF ABSTRACT ☐ UNCLASSIFIED/UNLIMITED ☒ SAME AS RPT ☐ DTIC USERS	21. ABSTRACT SECURITY CLASSIFICATION UNCLASSIFIED
22a. NAME OF RESPONSIBLE INDIVIDUAL Betty L. Fox	22b. TELEPHONE (Include Area Code) (202) 325-7042 22c. OFFICE SYMBOL DNA/STTI

DD FORM 1473, 84 MAR 83 APR edition may be used until exhausted.
All other editions are obsolete.

SECURITY CLASSIFICATION OF THIS PAGE
UNCLASSIFIED

PREFACE

The program supported under this contract consisted of the evaluation of emerging advanced composite materials for aircraft exposed to nuclear induced environments. The evaluation focused on two critical nuclear response characteristics: (1) thermal flash and (2) particulate (dust) erosion. Evolving composite materials for aircraft application were identified and various damage response mechanisms postulated. Materials were fabricated and various composite materials were evaluated analytically and experimentally in thermal and erosive nulcear generated environments. The results of these analyses are presented in two separate volumes under the single title NUCLEAR HARDNESS SIMULATION AND ANALYSIS OF COMPOSITE AIRCRAFT STRUCTURES, Defense Nuclear Agency Contract No. DNA 001-82-C-0245.

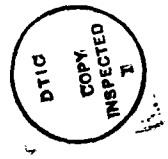

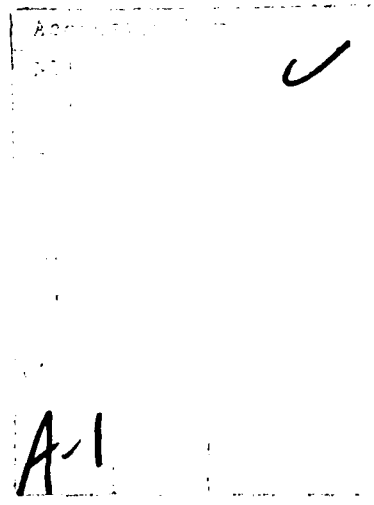

CONVERSION TABLE

Conversion factors for U.S. customary to metric (SI) units of measurement.

To Convert From	To	Multiply By
angstrom	meters (m)	1.000 000 X E -10
atmosphere (normal)	kilo pascal (kPa)	1.013 25 X E +2
bar	kilo pascal (kPa)	1.000 000 X E +2
barn	meter^2 (m^2)	1.000 000 X E -28
British thermal unit (thermochemical)	joule (J)	1.054 350 X E +3
calorie (thermochemical)	joule (J)	4.184 000
cal (thermochemical)/cm^2	mega joule/m^2 (MJ/m^2)	4.184 000 X E -2
curie	giga becquerel (GBq)*	3.700 000 X E +1
degree (angle)	radian (rad)	1.745 329 X E -2
degree Fahrenheit	degree kelvin (K)	$T_K = (t°\ f + 459.67)/1.8$
electron volt	joule (J)	1.602 19 X E -19
erg	joule (J)	1.000 000 X E -7
erg/second	watt (W)	1.000 000 X E -7
foot	meter (m)	3.048 000 X E -1
foot-pound-force	joule (J)	1.355 818
gallon (U.S. liquid)	meter^3 (m^3)	3.785 412 X E -3
inch	meter (m)	2.540 000 X E -2
jerk	joule (J)	1.000 000 X E +9
joule/kilogram (J/kg) (radiation dose absorbed)	Gray (Gy)**	1.000 000
kilotons	terajoules	4.183
kip (1000 lbf)	newton (N)	4.448 222 X E +3
kip/inch^2 (k/in^2)	kilo pascal (kPa)	6.894 757 X E +3
ktap	newton-second/m^2 ($N-s/m^2$)	1.000 000 X E +2
micron	meter (m)	1.000 000 X E -6
mil	meter (m)	2.540 000 X E -5
mile (international)	meter (m)	1.609 344 X E +3
ounce	kilogram (kg)	2.834 952 X E -2
pound-force (lbf avoirdupois)	newton (N)	4.448 222
pound-force inch	newton-meter (N·m)	1.129 848 X E -1
pound-force/inch	newton/meter (N/m)	1.751 268 X E +2
pound-force/foot^2	kilo pascal (kPa)	4.788 026 X E -2
pound-force/inch^2 (lb/in^2)	kilo pascal (kPa)	6.894 757
pound-mass (lbm avoirdupois)	kilogram (kg)	4.535 924 X E -1
pound-mass-foot^2 (moment of inertia)	kilogram-meter^2 ($kg·m^2$)	4.214 011 X E -2
pound-mass/foot^3	kilogram/meter^3 (kg/m^3)	1.601 846 X E +1
rad (radiation dose absorbed)	Gray (Gy)**	1.000 000 X E -2
roentgen	coulomb/kilogram (C/kg)	2.579 760 X E -4
shake	second (s)	1.000 000 X E -8
slug	kilogram (kg)	1.459 390 X E +1
torr (mm Hg, 0° C)	kilo pascal (kPa)	1.333 22 X E -1

*The becquerel (Bq) is the SI unit of radioactivity; 1 Bq = 1 event/s.
**The Gray (Gy) is the SI unit of absorbed radiation.

TABLE OF CONTENTS

LIST OF ILLUSTRATIONS

LIST OF ILLUSTRATIONS (Continued)

LIST OF TABLES

SECTION 1

INTRODUCTION

The susceptibility of advanced composite materials to solid particle erosion is becoming an increasing concern. Adler (1981) has indicated how laboratory erosion data can be used to predict the amount of material removed during flight through dusty environments. A very general model is available for making predictions of the mean depth of penetration (MDP) using relatively simple computational procedures. This model is described in Section 2. Once a suitable laboratory erosion data base is established, estimates of the MDP for a wide range of flight scenarios and component geometries can be made.

BMD Corporation (1984) has also provided estimates of the level of material removal that may occur for advanced composites in nuclear-generated dust environments, however, the material removal rates in this analysis are based on results for ceramic materials and are not directly related to non-metallic composites.

A survey of the solid particle erosion literature revealed that some experimental data is available for polymeric materials and fiber-reinforced, non-metallic composites. Although not directly applicable to the specific composites currently of interest, the available data (summarized in Section 3) is used to provide some initial insights into the magnitude of the erosion problem which may exist for advanced composite materials on aircraft flying through nuclear-generated dust. The dust distributions have been modeled by Yoon (1983). Using the published erosion data, the possibility exists for a significant amount of material removal to occur as shown in the examples presented in Section 4. Additional investigations are suggested in Section 5 to provide a more relevant estimate of the magnitude of the dust erosion problem and the possible enhancement of the damage which may occur by

encounters with rain environments. The experimental requirements for meaningful dust erosion assessments for aircraft are described in Section 6 where the capabilities of the existing facilities are summarized. A more general approach addressing dust erosion effects on composite aircraft structures is presented in Section 7. The magnitude of the test requirements and the analyses which have to be accomplished are clearly indicated.

The lack of meaningful data for evaluating the erosion of composite materials is a major obstacle to exercising the model described in Section 2. The estimates provided however do show that there could be a significant dust erosion effect for composite aircraft components. This is the primary conclusion (Section 8) resulting from this investigation.

SECTION 2

EROSION MODELING

The general structure of an erosion model which accounts for flight through a particulate environment, the shape of the component of interest, and the erosion rates for the material exposed to this erosive environment has been formulated by Adler (1979a, 1981). The primary features of this erosion model are described. The general forms of the data required for implementation of this erosion model are clearly established.

The mean depth of penetration (MDP) provides a measure of the material removal from an aircraft component during flight through a nuclear dust environment. The mean depth of penetration is determined as follows:

$$MDP[t] = \frac{M[t]}{\rho_T A} \tag{1}$$

where M[t] is the mass removed from the target material after an exposure time t in an erosive environment divided by the exposed surface area, A, and the density of the material, ρ_T. The mass removal for 90 μm silica sand impacting at 730 fps (500 mph) on a graphite fiber reinforced epoxy target as a function of the exposure time is shown in Figure 1. After a short incubation period (the nonlinear portion of the curve) a steady-state rate of material removal is achieved. This is a characteristic of the material removal process for moderate size particles at aircraft flight speeds. The subsequent evaluation of the erosion of aircraft components in nuclear-generated dust environments will be expressed in terms of the steady-state material removal rates. This approach provides a conservative estimate for the erosive losses which may result for arbitrary flight scenarios and component geometries.

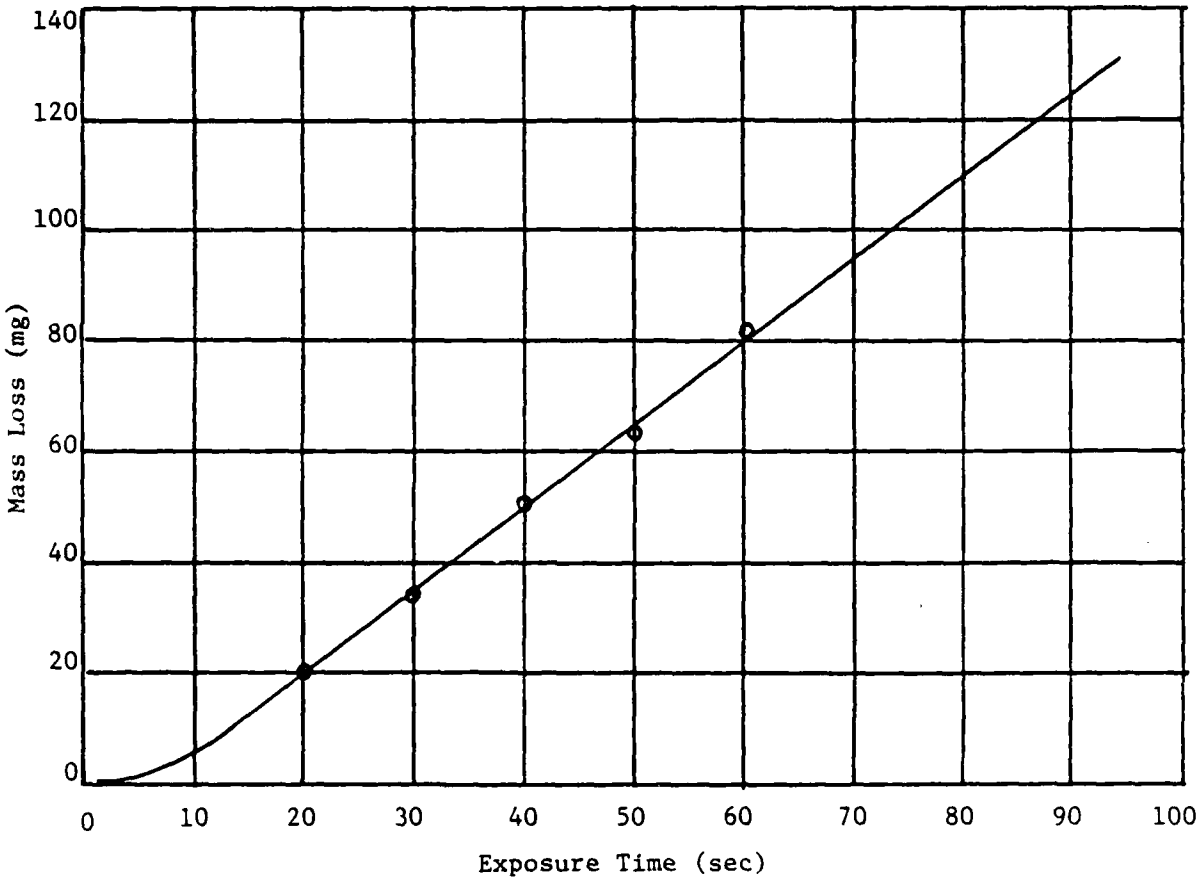

Figure 1. Mass loss for direct impacts of 90-micron sand on graphite-fiber reinforced epoxy at 730 fps (222 ms^{-1}) (Adler, 1973).

The basic measurement of the MDP defined in Equation (1) has to be generalized for the flight of aircraft through airborne dust. The MDP is now defined as the average depth of the amount of material removed from the aircraft component within a local region on the component. The cumulative effect of the material removed from all of the local regions comprising the entire exposed surface area of the component indicates the overall shape change of the component as a function of the time of flight in the dust environment. This generalized concept for the MDP can be expressed as

$$MDP = MDP\ [\underline{X},t;\ \underline{x},\ \tau;\ \Gamma_m] \tag{2}$$

where the parameters in brackets indicate the functional dependence of the MDP. The coordinates $\underline{X}$ denote the location of a specific region on the aircraft at a time t after the dust environment is encountered. The coordinates $\underline{x}$ denote the location of this areal element in space and the time τ is the aging of the dust environment at that location measured with respect to the initiation of the dust environment. The time t and the flight path $\underline{x}$ can be selected independently in order to evaluate the level of erosion damage which may be produced by the range of options available for penetrating the nuclear-generated dust environment.

The term Γ_m in Equation (2) is a representation for the variations in the composition of the lofted dust which may be encountered depending on the thermochemical changes which can occur within the fireball, the structural environment around the impact site, and the physics of the lofting process. The influence of the composition of the dust on its erosiveness is indicated as a factor which should be considered but explicit representations for its effects would have to be investigated in conjunction with studies of the dust environment.

The particle classification has to differentiate between angular or rounded solid particles, silica sand or soil, or rain. The additional parameters which influence the rate of material removal are explicitly identified in the relation which follows.

$$MDP = \frac{M}{\rho_t A}$$

$$= \frac{1}{\rho_t A} \sum_k \int_o^T \left(\frac{\text{mass loss } \left[\alpha_p^{(k)},\ v_p^{(k)},\ R^{(k)}; \underline{X},\ \Gamma_m \right]}{\text{unit mass of eroding particles}} \right)$$

$$\cdot \left(\frac{\text{mass of particles } [R^{(k)};\ \underline{x},\ \tau,\ \Gamma_m]}{\text{unit volume}} \right) \cdot$$

$$\cdot \left(\text{projected area} \perp \text{flight direction } [\alpha] \right) \cdot \underline{v}[\underline{x},t]\ dt \qquad (3)$$

where T is the total transit time and square brackets are used to indicate the designated quantity is a function of the parameters listed within those brackets. This relation simply states that the material removed from a specific location on the exposed surface of a component is equal to the material removed per unit mass of particles of a particular type multiplied by the total mass of particles of that type encountered during flight through a specified environment.

The conventional measure for solid particle erosion is the ratio of the mass of material removed to the mass of impacting particles: the erosion rate. The erosion rate is usually determined for steady state conditions, that is, the mass of material removed is unchanged for equal successive increments of eroding particles. The erosion rate is dependent on the type of particles encountered, the particle impact angle, α_p, the particle impact velocity, v_p, and the size of the impacting particle, $R^{(k)}$. The same definition of the erosion rate is

applicable to rain erosion except the erosion rate is generally a nonlinear function of time (or the number of drop impacts per unit area).

The designation of the particle sizes allows a distribution of particle sizes to be considered. The particle size distribution curve can be divided into N increments. If the increments, ΔR, are equal, although this is not necessary, then $R^{(k)}$ represents the mean size of the range $(R + (k-1)\ \Delta R) \leqslant R^{(k)} \leqslant (R + k\Delta R)$. The effect of particle size appears in the erosion rate as well as the particle concentration. The cumulative effect on mass removal is taken as a linear superposition (summation) of the damage associated with each particle size. This relation can be modified if the experimental data indicates this may be required.

A distinction is made in Equation (3) between the vehicle's velocity $\underline{v}$ and the velocity of the impacting particles $v_p^{(k)}$ for particles of mean radius $R^{(k)}$. This difference acknowledges that the particle/surface interaction due to the airflow over the component can modify the impact velocity of the particle. The same considerations apply to the particle impact angle $\alpha_p^{(k)}$ and the orientation α of the exposed surface.

If the exposed (local) surface area is not planar, it has to be divided into discrete areal elements due to the dependence of mass removal on impingement angle. Correspondingly Equation (2) can be rewritten in terms of the amount of material removed from each areal element.

$$MDP = \sum_i \frac{A^{(i)}[\alpha^{(i)}]}{A} MDP^{(i)} \tag{4}$$

where $MDP^{(i)}$ is the mean depth of penetration for the i^{th} areal element, $A^{(i)}$, comprising a particular component.

Introducing the symbol υ for the mass loss per unit mass and n for the mass of particles in a unit volume (particle concentration),

$$MDP^{(i)} = \frac{1}{\rho_t} \sum_j \sum_k \left\{ \frac{A_N^{(i)}[\alpha^{(i)}]}{A^{(i)}[\alpha^{(i)}]} \upsilon^{(ik)}\left[\alpha_p^{(ik)}, v_p^{(ik)} R^{(k)}\right] \cdot \right.$$

$$\left. \cdot n^{(k)} [R^{(k)}; \underline{x}, \tau] \underline{v}^{(j)}[x,t] \right\} \Delta t^{(j)} \qquad (5)$$

The notation $A_N^{(i)}[\alpha^{(i)}]$ signifies the projection of the area $A^{(i)}$ onto the plane normal to the flight direction. The time integral in Equation (5) is replaced with a summation. Time only occurs explicitly in connection with the vehicle velocity, since the steady-state erosion rates are assumed to be achieved for the dust environments and the particle concentrations are a function of the time elapsed from the onset of rainfall over a particular geographical area or the dust generated during a specific battlefield scenario. The establishment of the external environment is independent of the vehicle's time of flight.

A hemispherical dome will be used to demonstrate how the nonuniform material removal from a nonplanar component can be obtained from Equation (3). The areas in Equation (5) are evaluated explicitly for a hemispherical dome. Since the erosion rate depends on the impingement angle, the dome will be divided arbitrarily into ten equal radial segments as shown in Figure 2. Using the notation indicated in Figure 2, the i^{th} increment of exposed area of the target as a function of the impingement angle $A^{(i)}[\alpha^{(i)}]$ and the projection of this areal normal to the flight direction $A_N^{(i)}[\alpha^{(i)}]$ are determined from the following equations:

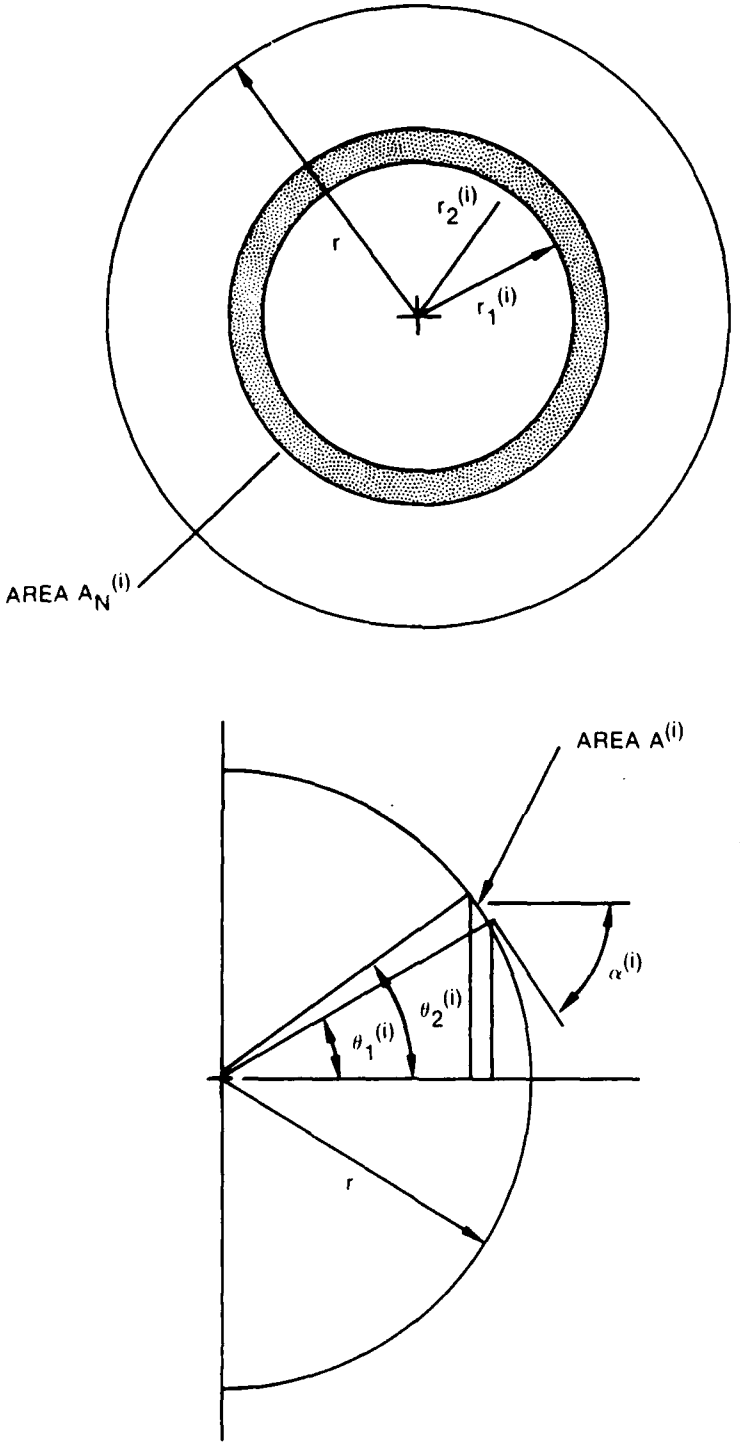

Figure 2. Geometry used for describing the erosion of a hemispherical dome.

$$A^{(i)}\left[\alpha^{(i)}\right] = 2\pi r^2 \left(\cos\theta_1^{(i)} - \cos\theta_2^{(i)}\right) \tag{6}$$

$$A_N^{(i)}\left[\alpha^{(i)}\right] = \pi r^2 \left(\sin^2\theta_2^{(i)} - \sin^2\theta_1^{(i)}\right) \tag{7}$$

The numerical values of the ten increments are tabulated in Table 1.

This discrete approach to the problem provides a suitable representation of the input data. A smooth curve can be drawn through the computed MDP data points as a function of dome angle. This curve should be a reasonable approximation to the actual dome contour after exposure to a defined environment and flight trajectory.

The flight trajectory is specified in terms of the velocity vector $\underline{v}$. During the course of the vehicle's flight various particle concentrations will be encountered. The particle concentrations will be functions of the vehicle's location in space denoted by the position vector $\underline{x}$. The time-dependent particle concentrations can be arrayed in a three-dimensional matrix representing the space of general interest as determined from representative dust and rain distributions.

The position and velocity vectors for the vehicle relative to some reference coordinate system, such as the local cartesian coordinates shown in Figure 3, are

$$\underline{x} = x_1\underline{e}_1 + x_2\underline{e}_2 + x_3\underline{e}_3 \tag{8}$$

$$\underline{v} = v_1\underline{e}_1 + v_2\underline{e}_2 + v_3\underline{e}_3 \tag{9}$$

The components of the velocity vector can be written

Table 1. Geometric parameters associated with a spherical dome.

i	$r_2^{(i)}/r$	$\theta_2^{(i)}$	$A^{(i)}/\pi r^2$	$A_N^{(i)}/\pi r^2$	$\alpha^{(i)}$
1	0.1	5°-44'	0.010	0.01	87°-8'
2	.2	11°-32'	.0304	.03	81°-22'
3	.3	17°-27'	.0516	.05	75°-30'
4	.4	23°-35'	.0750	.07	69°-29'
5	.5	30°-0'	.1010	.09	63°-12'
6	.6	36°-52'	.1320	.11	56°-34'
7	.7	44°-26'	.1720	.13	49°-21'
8	.8	53°-8'	.2280	.15	41°-13'
9	.9	64°-10'	.3284	.17	31°-23'
10	1.0	90°-0'	.8716	.19	12°-55'

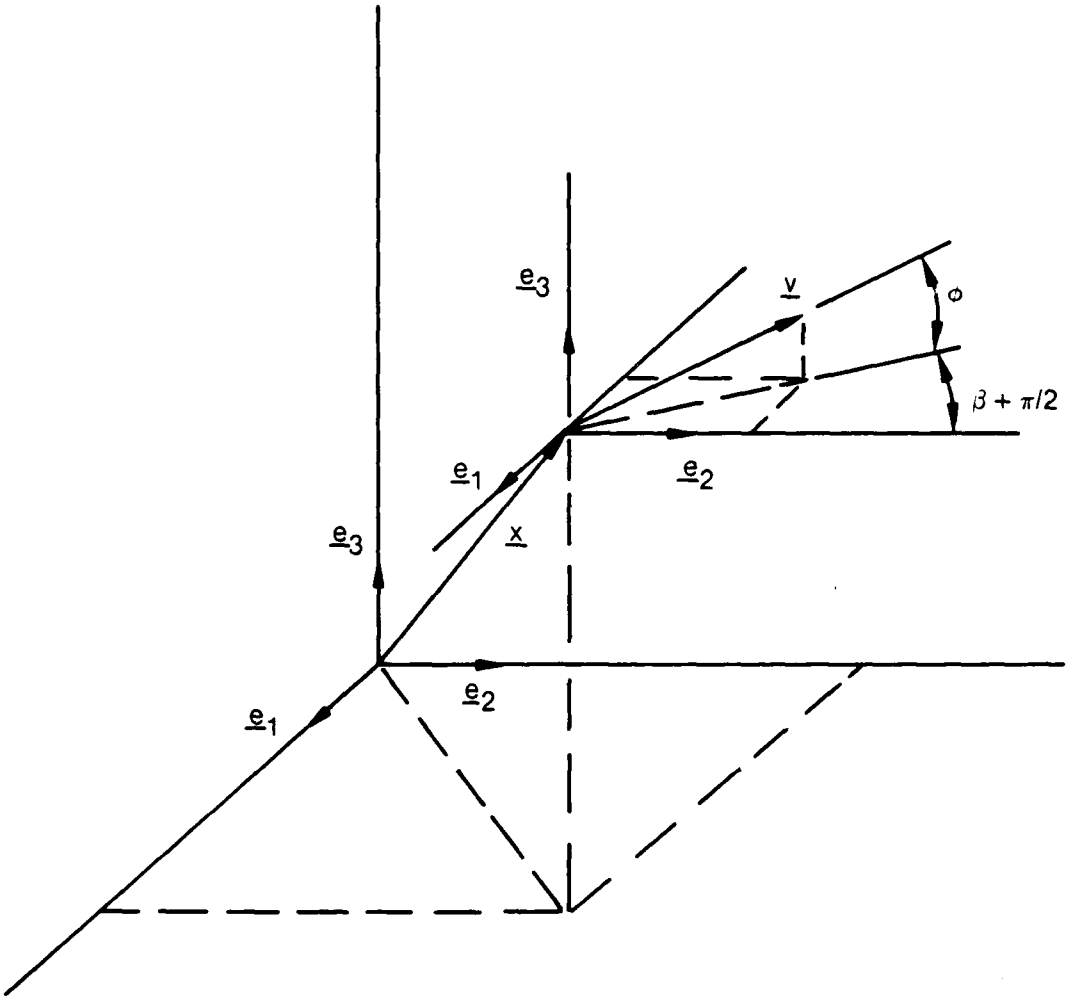

Figure 3. Specification of location and velocity of vehicle in space.

$$v_1 = v \cos\phi \cos\beta$$
$$v_2 = v \cos\phi \sin\beta \tag{10}$$
$$v_3 = v \sin\phi$$

The path of the vehicle is then given by

$$x_\ell^{(j+1)} = x_\ell^{(j)} + v_\ell^{(j)} \Delta t \tag{11}$$

where the subscript ℓ has the range 1,2,3.

The location of the vehicle in the environment can be evaluated from Equation (11) and the magnitude of the velocity vector $\underline{v}$ is determined from Equation (9). For numerical evaluations it is reasonable to replace the time integration in Equation (3) by a summation which equals the total length of the path the vehicle follows in space as indicated in Equation (5).

Although the velocity of the particles in a unit volume at some location in space does not appear explicitly in the particle concentration in Equation (5), it is essential to know the average particle velocity as a function of particle size and location in space in order to evaluate the relative particle impact speed $v_p^{(jk)}$. The initial particle velocity is denoted by $\underline{v}_o^{(k)}\ [\underline{x},\ R^{(k)}]$. The velocity vector for the particle of size $R^{(k)}$ impacting the vehicle at a location $\underline{x}$ in space is then determined from

$$\underline{v}_p^{(jk)} = \underline{v}^{(j)}\ (\underline{x}) + \underline{v}_o^{(k)} \left[\underline{x}, R^{(k)}\right] + \underline{v}^b \left[\underline{v}^{(j)}, \underline{v}^{(k)}, R^{(k)}\right] \tag{12}$$

where $\underline{v}^{(j)}$ is the velocity of the vehicle determined from the flight trajectory,

$\underline{v}_o^{(k)}$ the velocity of the particles prior to interacting with aerodynamic flows over the aircraft as determined

from numerical computations of the dust distribution, and

$\underline{v}^b$ has to be evaluated from an analysis of the particle interaction with the flow field around the vehicle.

The impingement angle $\alpha^{(ik)}$ can be determined from the velocity vector $\underline{v}^{(jk)}$ relative to the surface element whose normal vector is in the direction $\pi/2 - \alpha^{(i)}$.

The expression in Equation (5) is quite general and suitable for digital analysis. Using a computer the material removal rates can be evaluated at various locations on a component of irregular shape for specified flight trajectories through temporally changing particulate environments. Once the vehicle trajectory is established, it is necessary to prescribe $\upsilon^{(ik)}$ using erosion test data and $n^{(k)}$ to describe the environment. It is important to note that the erosion data does not change; only the manner in which it is utilized in evaluating the MDP will change. Once tests have been carried out for a material of interest, for a range of impact angles, impact velocities, particle sizes, and particle types, this data base, if broad enough, can be used to evaluate the erosive effects for any of the operational environments which may be encountered.

There are many factors which influence the material removal process; however the particle size exponent and the velocity exponent will be of primary concern, since these parameters are common to the majority of the particle erosion analyses which can be found in the literature. The lack of agreement between the results of the theories based on kinetic energy exchange between the impacting particle and the target has been a perplexing issue in the field of solid particle erosion. The general form of the expression for volume removal (volume removed per particle impact) can be written,

$$\upsilon = g\, v_p^a\, R^b f(\alpha_p) \tag{13}$$

where g is a functional representing the dependence on all of the *parameters not explicitly stated and*

v_p is the particle impact velocity
R is the mean radius of the impacting particle
$f(\alpha_p)$ is a function of the attack angle α_p
a is the velocity exponent
b is the particle size exponent.

The velocity exponent has been generally found to range from two to three for materials displaying ductile behavior for a wide range of particle impact conditions, however exponents (up to 4) have been obtained by Grant and Tabakoff (1975) and Tabakoff, et al (1979). Tabakoff's results are based on detailed observations of the aerodynamics of the particle flow and the rebound characteristics of the particles impacting the eroding surface of the target. The velocity exponents for brittle materials range from 1 to 6.5 (cp. Gulden, 1979a; Sargent, et al., 1979). The velocity exponent depends on the size, material, shape, and angle of attack of the impacting particle, however it does not appear to be significantly affected by the microstructure of the target material.

The particle size exponent has not been adequately evaluated. It is generally stated that the volume removal in metals is independent of particle size for particle sizes in excess of 100 μm (Tilly, 1969). The variations in particle size effects have already been noted for smaller particle sizes in brittle materials (Sheldon and Finnie, 1966). Gulden's test data (Gulden, 1979a,b) shows $b \simeq 4$ for magnesium fluoride impacted by quartz particles, however hot-pressed silicon nitride impacted by silicon carbide particulates displayed a $b=4$ dependence while impacts by quartz produced a $b=3$ dependence as well as a change in $a=4$ to $a=1$ for particle sizes from 8 to 940 μm. A definite threshold for achieving an $R^4 V_o^4$ relation was found for reaction-bonded silicon nitride impacted by quartz particles. The above results are for normal

impacts on the target surface. The dependence of the particle size exponent on the particle material is evident, but it is not known how it would vary with the angle of attack.

The complete characterization of a particular impact condition (particle impact type and target material) involving the particle size, impact velocity, and impingement angle requires numerous erosion tests. Thus a reliable experimental data base for the development as well as comparison of analytical results is rarely found in the particle erosion literature which leaves many aspects of the subject unsettled. The analytical approaches which have been undertaken to describe material removal due to both solid and liquid particle erosion have been described and evaluated by Adler (1979b,c).

SECTION 3

SOLID PARTICLE EROSION OF COMPOSITE MATERIALS

Experimental evaluations of the material removal rates for polymeric and composite materials are summarized in Table 2. This is all of the data which could be found in the open literature. Some general observations concerning this data are provided.

A somewhat more extensive data base exists for rain erosion evaluations of polymeric materials than for solid particle erosion. However it is important to note that, while attempts have been made to correlate the data generated in each of these environments, little correspondence exists between the respective material removal rates. Thus, based on the author's experience related to both solid particle and rain erosion evaluations, it is not possible to use rain erosion data to predict the erosion rates for solid particle impacts (Adler, 1979a).

Setting this issue aside, the solid particle erosion investigations summarized in Table 2 will be used as the data base for estimating the material removal rates for potential nuclear dust environments. The recent work of Zahavi and Schmitt (1981a,b) is of interest, but the particle impact velocities (about 42 ms^{-1}) are too low to provide relevant material removal rates.

There are some general trends in the solid particle erosion data which remain to be established for fiber-reinforced composites. For ductile metals the steady-state erosion rates become constant with respect to particle size beyond a certain particle size (on the order of 100 μm); the critical particle dimension is dependent on the particle type and impact velocity (Goodwin, Sage and Tilly, 1969; Tilly and Sage, 1970). This limitation does not appear to be applicable to glass which is representative of brittle response. The maximum (steady-state)

Table 2. Summary of test data for solid particle erosion of composite materials.

Reference	Material	Particle Material	Particle Size (mm)	Test Apparatus	Velocity Range (ms^{-1})	Impact Angle
Behrendt (1974)	GFRP 180/37%	SiO_2-	0.2 to 0.25	Rotating arm	100-400	30 to 90°
	Astrocoat on GFRP	SiO_2-	0.1 to 0.125			90°
			0.2 to 0.25		250	30 to 90°
			0.3 to 0.4			90°
	GFRP + 400 μm Fluorocarbon coating	SiO_2-	0.2 to 0.25		250	90°
Williams and Lau (1974)	GFR epoxy (unidirectional graphite)	SiO_2-rounded	0.044 to 0.250	unknown	47-109	90°
		SiO_2-rounded	0.077 to 0.125		70	30 to 90°
Tilly and Sage (1970)	Polyurethane	SiO_2-angular	0.125 to 0.150	Rotating arm	128	90°
	Nylon (Type 66)				60-305	90°
	Glass-reinforced nylon 30% glass fiber in Type 66					
	Carbon-reinforced nylon 25% carbon fiber in Type 66					
	Fiberglass 70% glass in epoxy					
	Polypropylene					
Tilly (1969)	Nylon (Type 66)	SiO_2-angular	0.06 to 0.125	Air blast	104	40°, 90°, 70 to 90°
	Carbon-reinforced nylon 25% carbon fiber in Type 66					
	Glass-reinforced nylon					
	Fiberglass 70% glass in epoxy					
	Polypropylene					
Adler (1973)	GFR 31 w/o Epoxy (unidirectional)	SiO_2-angular	0.090	Rotating arm	222	90°
Hanavi and Schmitt (1981a)	Glass-reinforced polybutadine	SiO_2-rounded -elongated	0.210 to 0.297	Air blast	42	30° to 90°
	Glass-reinforced polyimide					
	Glass-epoxy laminates Typically 35% resin, 65% reinforcement					
Hanavi and Schmitt (1981b)	Coatings - Polyurethane (MIL-C-83286)	SiO_2	0.210 to 0.297	Air blast	42	15° to 90°
	Polyurethane (MIL-C-83231)					
	Fluorocarbon (AF-C-MBW-15-15)					

erosion rate for ductile metals occurs at an impact angle around 20°, while normal (90°) particle impacts are the most damaging for brittle materials. For very small particles (c 10 μm) the maximum erosion rate for brittle ceramics shifts to impact angles less than 90° (Sheldon and Finnie, 1966).

The trends in the erosion rates for polymeric composites are dependent on the specific composite material being evaluated and are typically intermediate to the general trends observed for ductile and brittle materials. For polymeric composites there is a tendancy for a mass increase for certain impact conditions (as normal incidence is approached) due to particle embedding rather than mass removal during the initial stages of the erosion process.

Details of the experimental apparatus and procedures used are relatively scant in the published reports along with the test procedures used. The limited information that is available will be used to reconstruct the manner in which the stated results were obtained.

Tilly and his co-workers (Tilly, 1969; Tilly and Sage, 1970) used both a sand blast apparatus and a rotating arm test configuration as indicated in Table 2. The rotating arm provided impact velocities more representative of those encountered in gas turbines operating in dusty environments, while the sand blast apparatus was used to obtain elevated temperature data. A single specimen was mounted at each end of a 10.16 cm (4 in.) arm and for higher velocities (approaching 550 ms^{-1}) a 15.24 cm (6 in.) arm. Sand was dropped from a dispenser at one point along the circumference of the circle through which the specimen passed. The height of fall of the sand could be adjusted so that all of the sand impacted the specimens. Tilly indicates that at most 7% of the sand released may miss the specimens. The specimens were 1 cm (0.4 in.) squares machined with a shank for attachment to the rotating arm. It is assumed that the polymeric samples were fastened to a metal backing in order to obtain mass loss data for these materials. In the sand blast

device the particle-laden air stream was directed at the central portion of the specimen. The quantity of particles impinging the specimen is taken to be proportional to the projected area of the test specimen normal to the flow.

The AFML/Bell rotating arm erosion facility (Adler, 1973) has a rotating arm which places the specimen at a radial distance slightly greater than 2.75 m (9 ft). The short arm radius used by Tilly did not let the particles fall the width of the specimen before they were impacted again. The large radius of the Bell arm allows the particles to fall more than 30 cm before they are impacted on the next revolution of the arm. The Dornier System's rotating arm (Behrendt, 1974) has a radius of 1.2 m (3.94 ft). No information is provided in the paper by Williams and Lau (1974) as to the apparatus or procedures which were used to obtain the data reported.

The actual number and condition of the particles striking the specimens in these erosion facilities are typically determined indirectly. Adler (1973) calculated the number of impacts for the AFML/Bell rotating arm using the following relation for the test arrangement shown in Figure 4,

$$N_I = \frac{N}{720\sqrt{2gh}} \frac{\ell}{\ell'} d' \cos\theta \qquad (14)$$

where N_I is the number of particle impacts the specimen experiences per revolution of the rotating arm,

N is the number of particles released into the path of the specimen per minute,

$\sqrt{2gh}$ = 21.233 fps for the AFML/Bell erosion facility,

ℓ is the lateral dimension of the sand ejection nozzle,

ℓ' is the lateral dimension of the exposed area on the specimen's surface in inches,

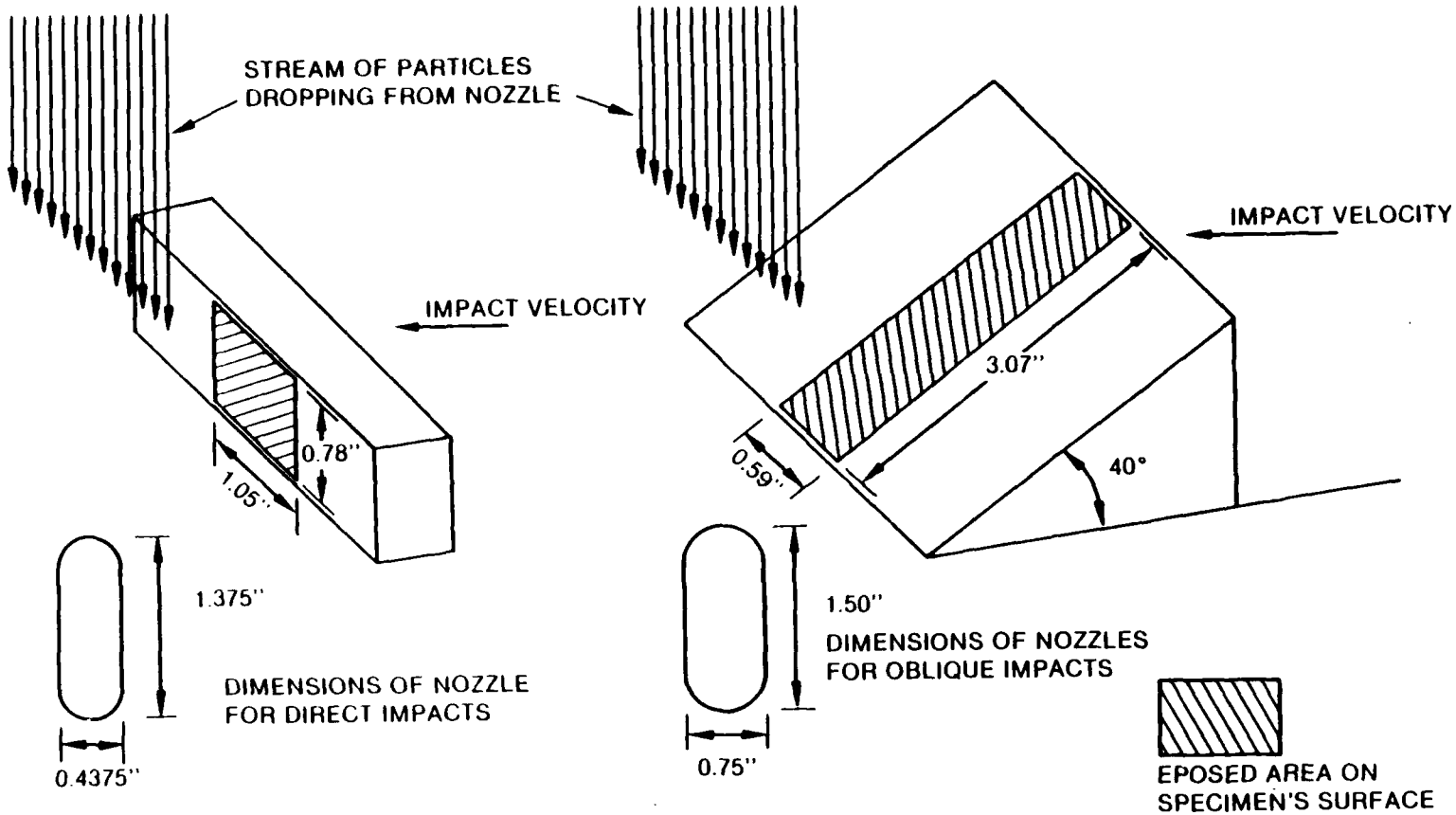

Figure 4. Nozzle dimensions and experimental arrangement for direct and oblique solid particle impacts in the AFML/Bell Rotating Arm Facility (Adler, 1973).

d′ is the transverse dimensions of the exposed area on the specimen's surface in inches.

The specimen used in Adler's experiment was a half cylinder: 1.27 cm (0.5 in.) diameter x 5.08 cm (3 in.) long. The erosion rates with this geometry represent a range of impact angles which distorts the values obtained. For normal impacts, $\theta = 0°$ as defined here, $\ell = 1.375$ in., $\ell' = 2.5$ in., and $d' = 0.5$ in. Since ℓ' is greater than ℓ, the ratio ℓ/ℓ' is taken to be unity; however, the particle spray expands as it exits from from the nozzle, so deviations from the ideal conditions do occur. The nominal 90 μm quartz sand was dispensed at a rate of 260 g/min. The particle size distribution is shown in Figure 5 and is skewed to the larger particle dimensions. Assuming an equivalent spherical diameter of 90 μm and a density for quartz of 2.2 g/cc, the value of N in Equation (12) is determined to be 3.10×10^8 particles/min. Using these values in Equation (12) yields a value of $N_I = 9.30 \times 10^3$ particles/rev. At $v_p = 222$ ms^{-1} (730 fps) the RPM for the AFML/Bell arm is $1.05\ v_p$ or 766. The particle impacts per second are then estimated to be 1.19×10^5. This value can be used with the measured mass loss per exposure increment in Figure 1 to obtain an approximation of the erosion rate. It is again important to note that the specimen was a half-cylinder and so the erosion rate in Table 2 cannot be reliably associated with a single impingement angle. With this reservation $\alpha_p = 90°$ will be assigned for the initial evaluation.

Behrendt (1974) does not provide explicit information on how the mass of impacting particles was obtained, so it is not possible to evaluate the consistency in the erosion rates he obtained and those obtained by other investigators using rotating arms. Behrendt's erosion evaluations are moderately extensive providing the variations of erosion rates with impact velocity and impact angle as shown in Figure 6 to 8 for a graphite fiber reinforced composite (the exact constituents are not specified). The samples are cylindrical with a 16.8 mm (0.66 in.) diameter and a thickness of 2.5 to 5.0 mm (0.1 to 0.2 in.).

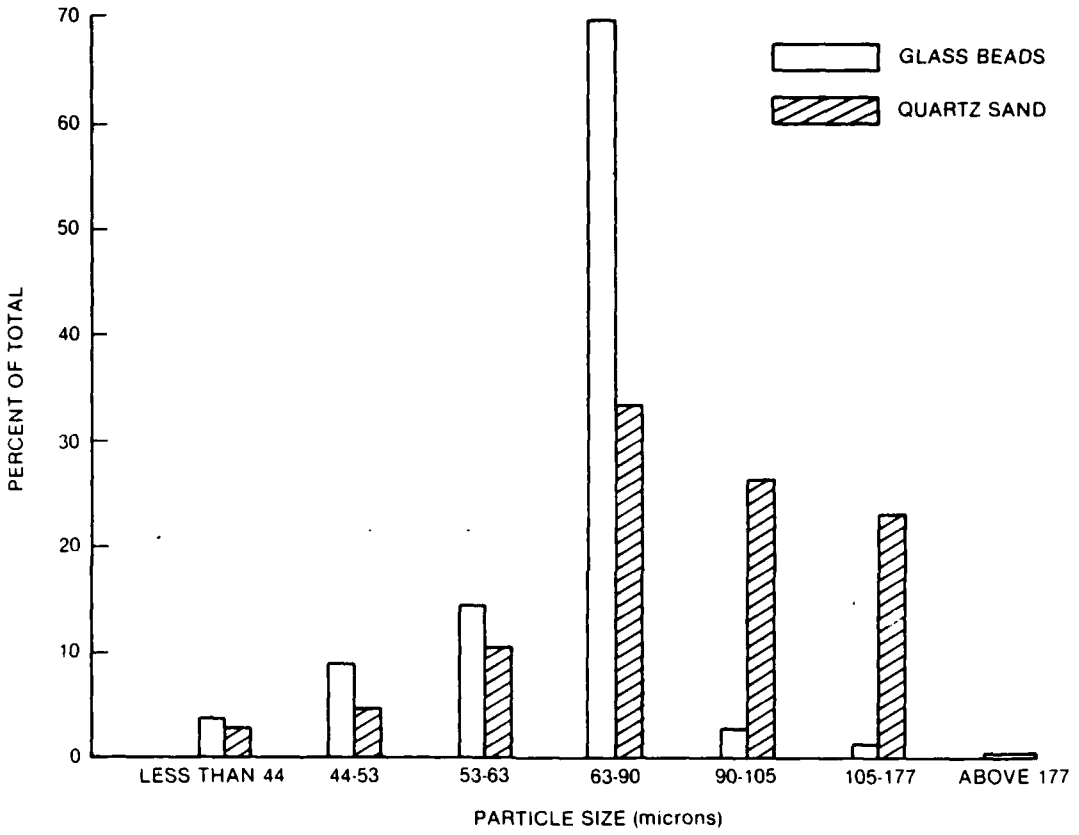

Figure 5. Particle size distributions for 70-micron glass beads and 90-micron sand (Adler, 1973).

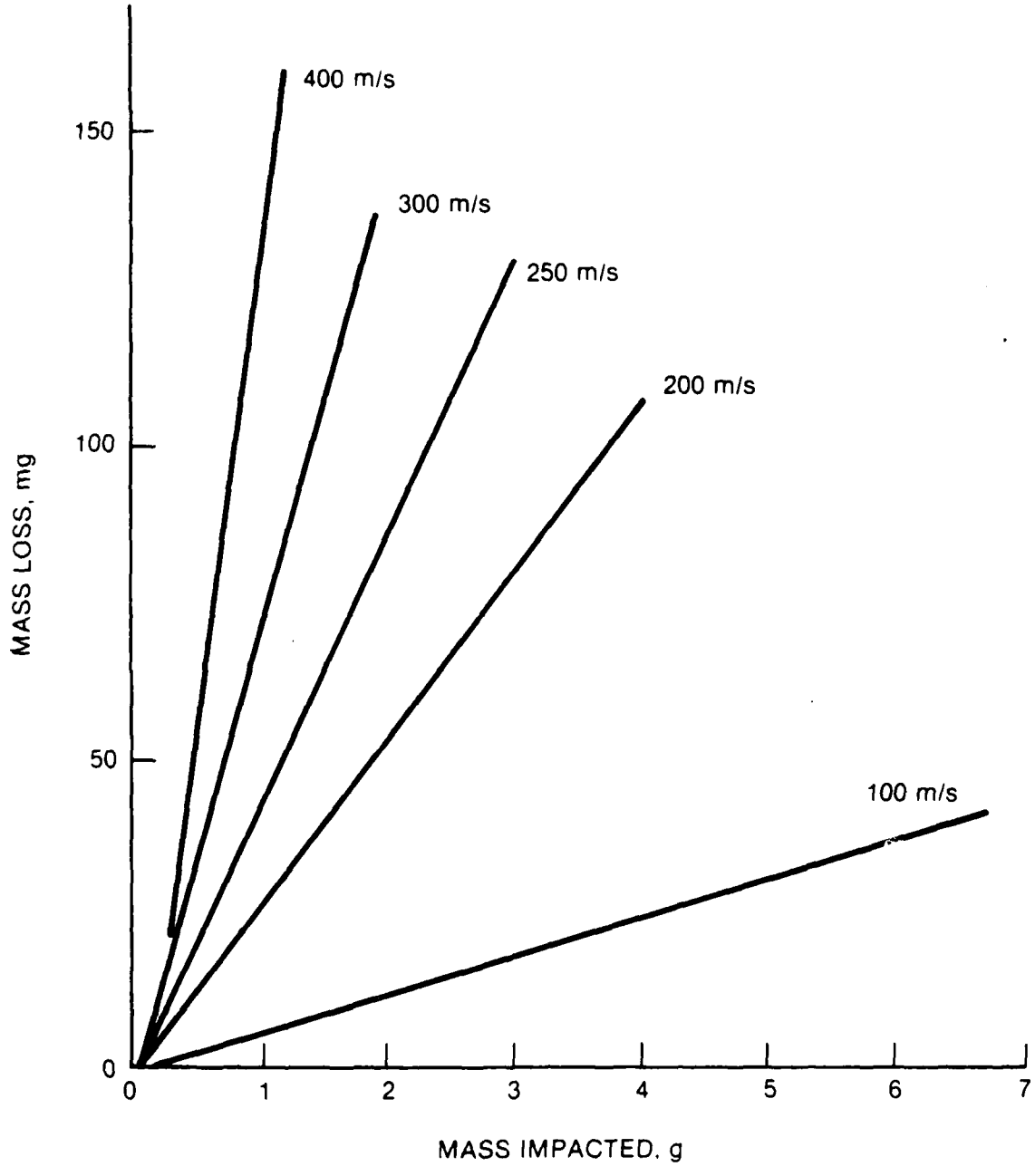

Figure 6. Material removal rates for a graphite-fiber reinforced epoxy (Behrendt, 1974).

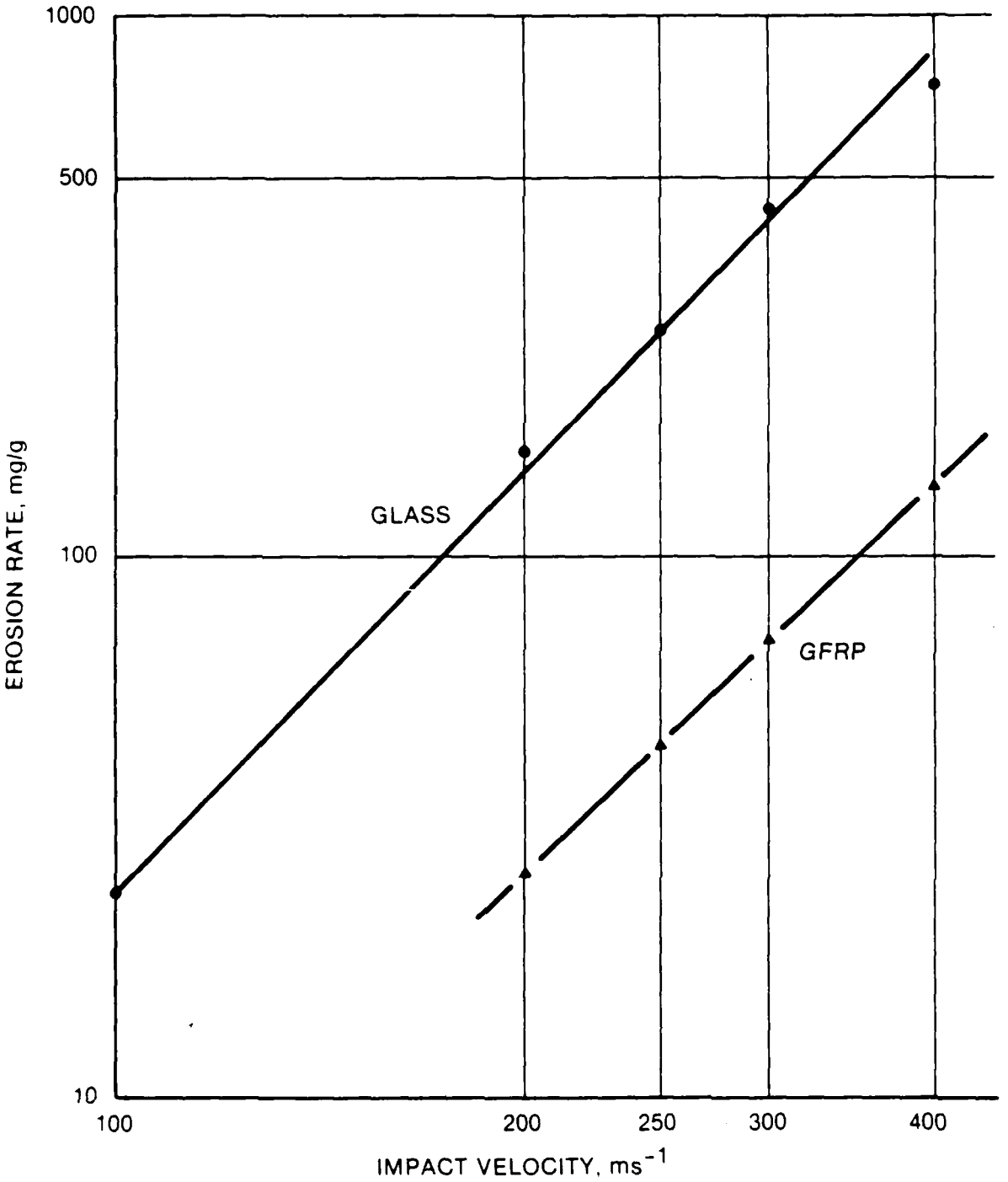

Figure 7. Steady-state erosion rates for graphite-fiber reinforced epoxy as a function of particle impact velocity (Behrendt, (1974).

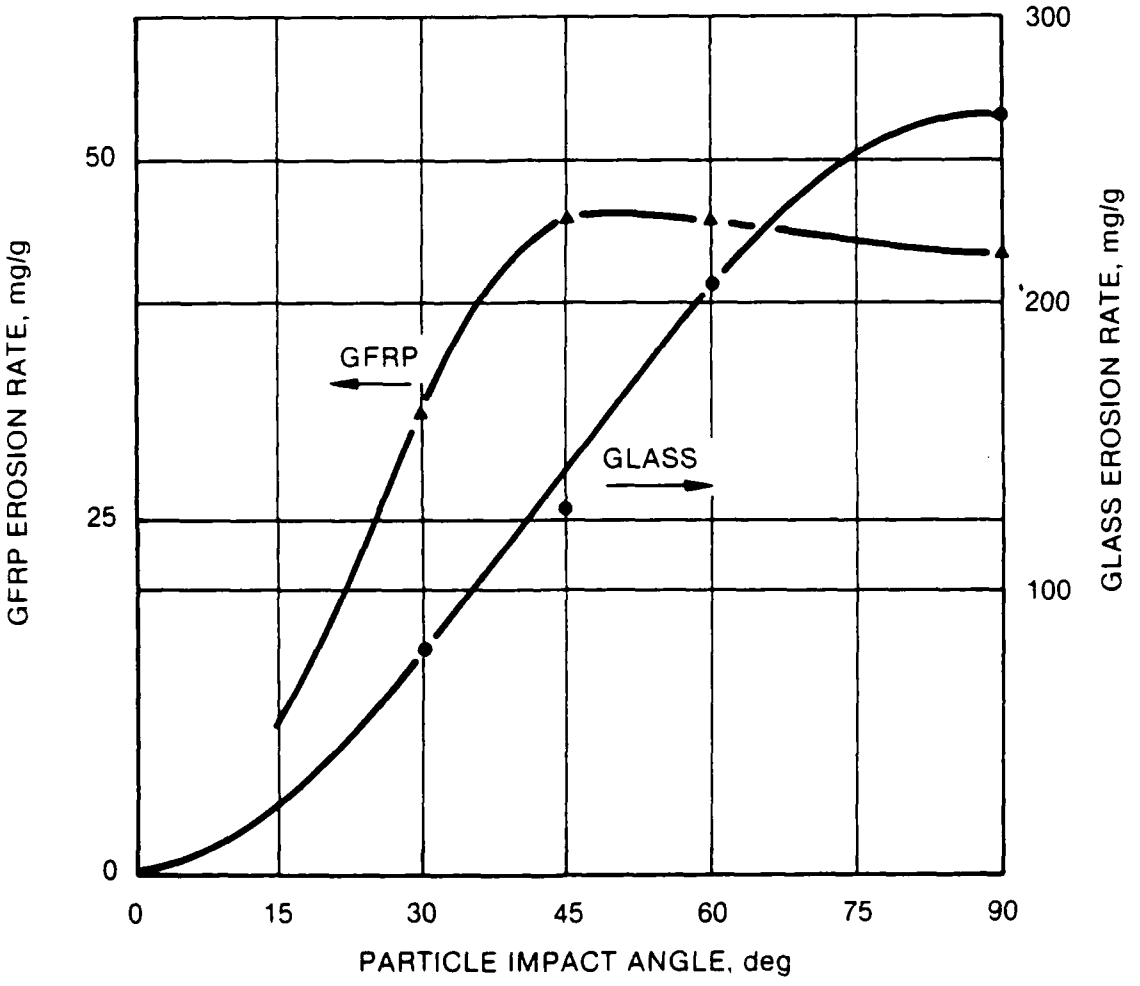

Figure 8. Variation of erosion rate with particle impact angle (Behrendt, 1974).

The dependence of the erosion rate on the impact parameters was defined in Equation (13).

$$\upsilon = g\, v_p^a\, R^b\, f(\alpha_p)$$

where g is a functional representing the dependence on all of the parameters not explicitly stated, a is the velocity exponent, and b is the particle size exponent. Behrendt's results indicate that $a \simeq 2.4$ and the functional dependence on α_p at 250 ms^{-1} can be obtained from Figure 8. The maximum erosion rate occurs at an impact angle of 45°. On the other hand, Williams and Lau (1974) find from their experiments that

$$\upsilon = 0.01\ (2R)^{0.9}\ [v_p \sin\ (\alpha_p + 24°)]^{3.4} \qquad (15)$$

This expression is based on 100 μm quartz particles impacting unidirectional graphite fiber reinforced epoxy speciment at 70 ms^{-1} (230 fps). The maximum erosion rate for the test conditions used by Williams and Lau occurs at an impact angle of 65° (Figure 9). It is also important to note that the velocity exponent in Equation (15) is 3.4 which is considerably higher than that found by Behrendt (1974) but the impact velocity is quite low.

Tilly and his co-workers (Table 2) find that the erosion rate for nylon and glass carbon fiber reinforced nylon has a maximum at an impingement angle of 30° (Figure 10). Quartz particles ranging from 60 to 125 μm sieve diameters imparted the specimens at v_p = 104 ms^{-1} (341 fps). Tilly demonstrated that a significant mass of quartz particles had to impact the polymeric test samples before the erosion rates would begin to approach their steady-state values. This effect is greater for 90° impacts than for 40° collisions (Figure 11). 400g of quartz particles were used to obtain the erosion rates in Figure 10, however, according to Tilly's evaluation of the influence of the mass of the

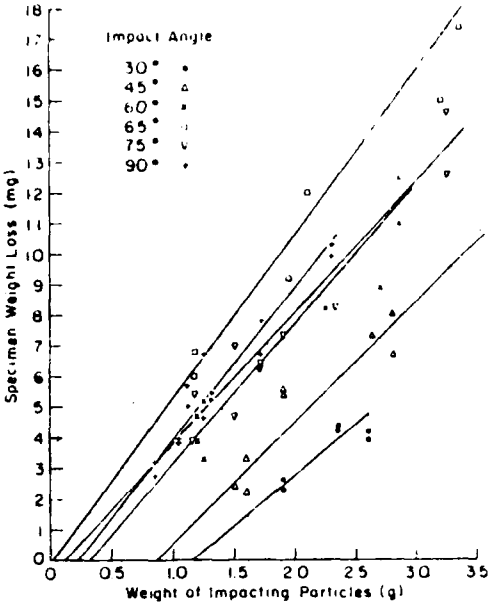

(a) Weight loss of graphite-epoxy composite for varying impact angle. (Particle velocity = 70 m/s and particle size range = 77-125 μm).

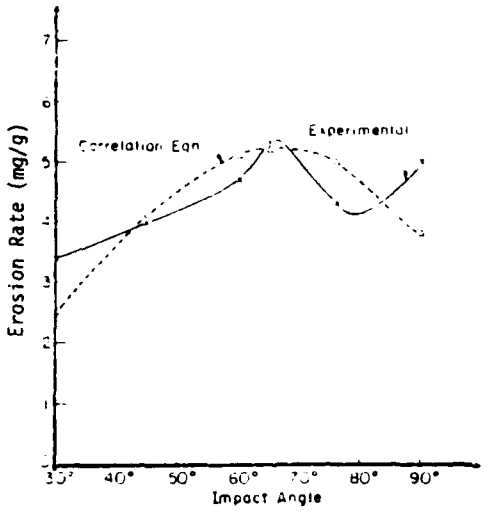

(b) Correlation Equation and Experimental Results.

Figure 9. Erosion behavior of graphite-fiber reinforced epoxy (Williams and Lau, 1974).

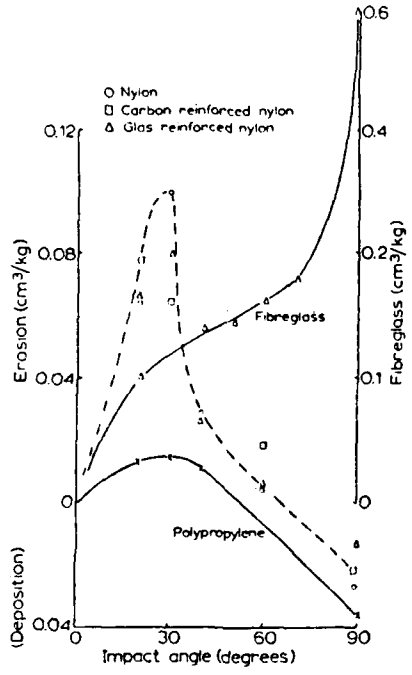

Figure 10. Variation of erosion rates for polymeric materials with impact angle (Tilly, 1969).

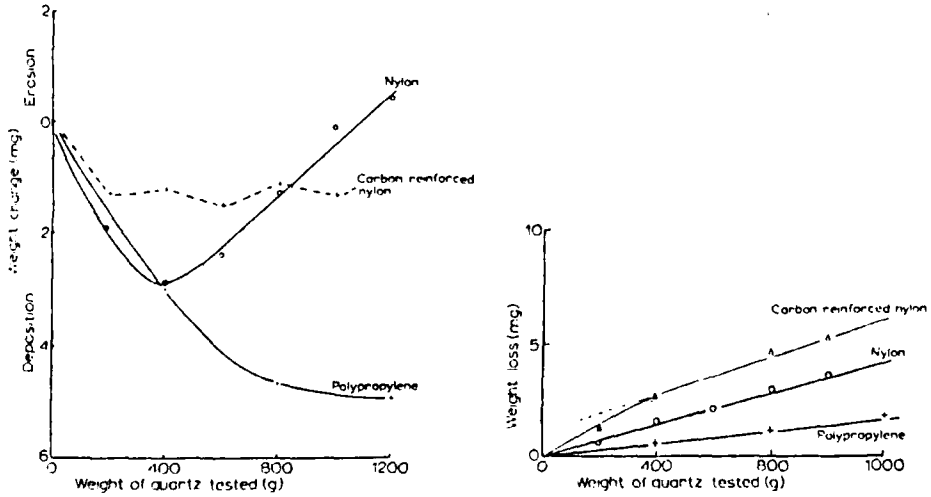

Figure 11. Variation of weight loss with quantity of abrasive for polypropylene and nylon (Tilly, 1969).

impacting particles, the erosive response is still not stabilized for 400g of quartz particles. This observation raises doubt as to the accuracy of the data reported in Figure 10. In addition the data points are not sufficient to confirm that the results for nylon, carbon-reinforced nylon, and glass-reinforced nylon are nearly identical in the vicinity of $\alpha = 30°$ (Figure 10). For a fairly broad range of materials, Tilly and Sage (1970) found that the velocity exponent was approximately 2.3 for normal impacts of 125 to 150 μm quartz particles impacting from 60 to 300 ms^{-1} as can be seen in Figure 12.

The erosion rates, υ, which can be determined from the publications described above are summarized in Table 3 for the particle impact conditions which are of interest for assessing aircraft vulnerability to nuclear-generated dust. Although a sizable increase is seen in the erosion rates at intermediate impact angles at low impact velocities (as shown in Figure 10), the difference between the maximum erosion rate at an intermediate angle compared to normal collisions may not be as drastic at impact velocities in the vicinity of Mach 1 (as indicated in the plot in Figure 8). The values of υ for normal impacts in Table 3 will therefore be assumed to be slightly low but indicative of the maximum erosion rates.

In order to convert the volumetric erosion rates reported by Tilly and Sage (1970) to mass loss per unit mass of impacting particles, the densities of the composites they evaluated have been estimated. These estimated densities are indicated in Table 3. The composite materials are all quite different, so the available data can only be used to provide a very crude estimate of the solid particle erosion rates current composite materials may experience for better defined erosive conditions. The erosion rates from Tilly and Sage (1970) show the range of values that may occur, however the graphite-fiber reinforced epoxy data obtained by Adler (1973) and Behrendt (1974), which may be more representative of present day composites, will be used to obtain some idea of the MDPs for aircraft flying through nuclear-generated dust environments.

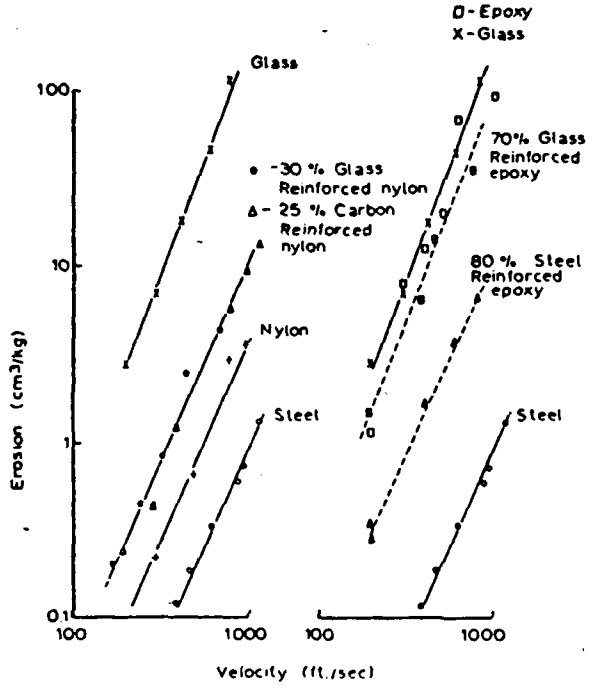

Figure 12. Velocity dependence of composites tested with 125-150 μm quartz at 90° (Tilly and Sage, 1970).

Table 3. Erosion rates for quartz particles impacting composite materials at normal incidence.

Source	Material	Particle Size (mm)	Impact Velocity (ms^{-1})	Erosion Rate (mg/g)
Tilly and Sage (1970)	30% glass fibers in type 6,6 nylon $\rho \approx 1.56$ g/cc.	125-150	185	4.93
			245	10.9
			305	17.14
	70% glass fibers in epoxy (fiberglass) $\rho \approx 2.05$ g/cc.		185	53.5
			245	109.
			305	170.
	25% carbon fibers in type 6,6 nylon $\rho \approx 1.28$ g/cc		185	4.05
			245	9.00
			305	14.06
	Type 6,6 nylon $\rho \approx 1.16$ g/cc		185	1.28
			245	2.67
			305	4.53
Behrendt (1974)	GFRP 180/37%	200-250	100	6.08
			200	26.4
			250	43.5
			300	70.8
			400	137.7
Adler (1973)	31 v/o graphite in epoxy	90	222	19.10

The dust distributions (Yoon, 1983) are specified in terms of the particle size. Unfortunately the erosion rates obtained by Adler (1973) and Behrendt (1974) are for a single mean particle size, so it is quite difficult to specify the variations of υ with particle size. Several forms of the dependence of υ on particle size are likely to exist based on the trends in the solid particle erosion response of other materials. The available data is plotted in Figure 13 as a function of the mean particle size. The range in the form of the dependence of υ on particle size is indicated in Figure 13. At this time it is not possible to select one form over another, but the data deficiency could be eliminated with a small experimental effort. It was stated at the beginning of this section that the steady-state erosion rates for ductile metals become constant with respect to particle size, however the erosion rates for more brittle materials may not display this same effect but may tend to increase for a considerably larger range of particle dimensions. These two possibilities are reflected in the erosion rates for the smaller particle dimensions.

The solid particle erosion rates for non-metallic composites obtained from the existing literature, be that what they may, will be used in Section 4 to provide very preliminary estimates of the removal rates for hypothetical aircraft trajectories traversing the continental United States.

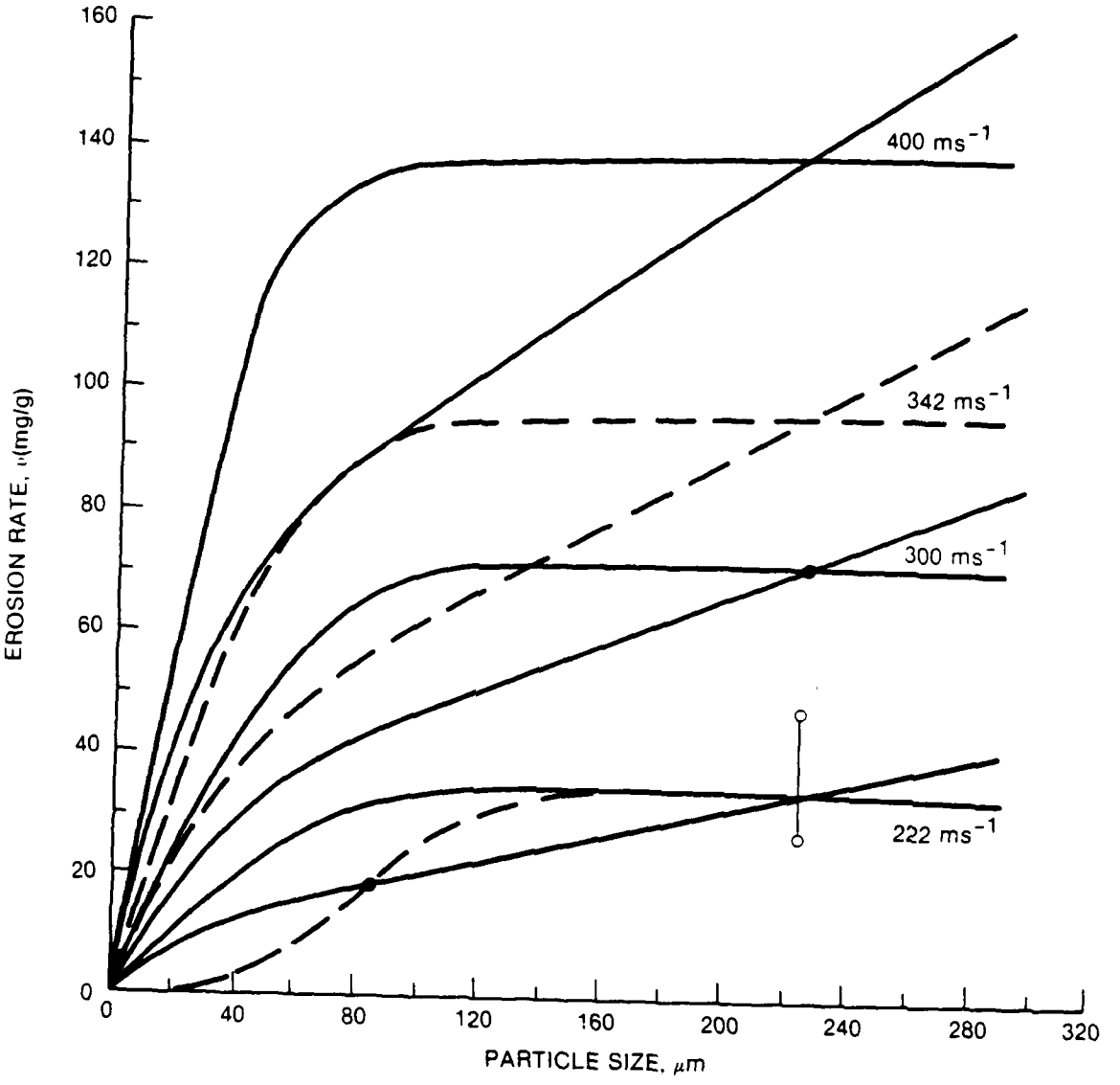

Figure 13. Estimated erosion rates as a function of particle size for 90° impacts.

SECTION 4

MASS REMOVAL ESTIMATES

The extent of the damage which may result from flight through nuclear-generated dust will be estimated using the erosion model described in Section 2 and the extrapolations of the experimental erosion rates summarized in Section 3. The specific conditions to be evaluated are the hypothetical deployment of aircraft from the southwestern United States at various times after a nuclear attack on missile sites within the continental United States.

The general relation in Equation (5) will be evaluated using the dust distributions calculated by Yoon (1983). Representative dust distribution plots are available as shown in Figures 14 to 16. Two trajectories passing through the dust fields have been selected for aircraft flying across the continental United States without consideration of how realistic they might be. These trajectories will be used to demonstrate how the temporal development of the dust fields can be introduced into the erosion model to evaluate the MDP. The two trajectories labeled A and B are superposed on the dust distributions in Figures 14 and 16. Since only a limited number of time increments have been computed for the dust distribution, the evaluation of Equation (3) has to be carried out for a much larger time increment (essentially a static dust distribution) than would be the case if the model could be adequately implemented. A more reasonable time increment for these dust distributions would be $\Delta t = 100$ sec. for an aircraft flying at 300 to 400 ms^{-1}. The aircraft would fly roughly 20 nmi during this time increment for a flight speed of 375 ms^{-1} (c.750 knots). It would also be desirable to have the dust concentrations isocontours at intervals of 3, 15, 30, 45, 60, 90, 120, and greater than 150 mg/m^3.

The dust field calculations (Yoon, 1983) provide the mean and range of particle sizes in the atmosphere as a function of time after

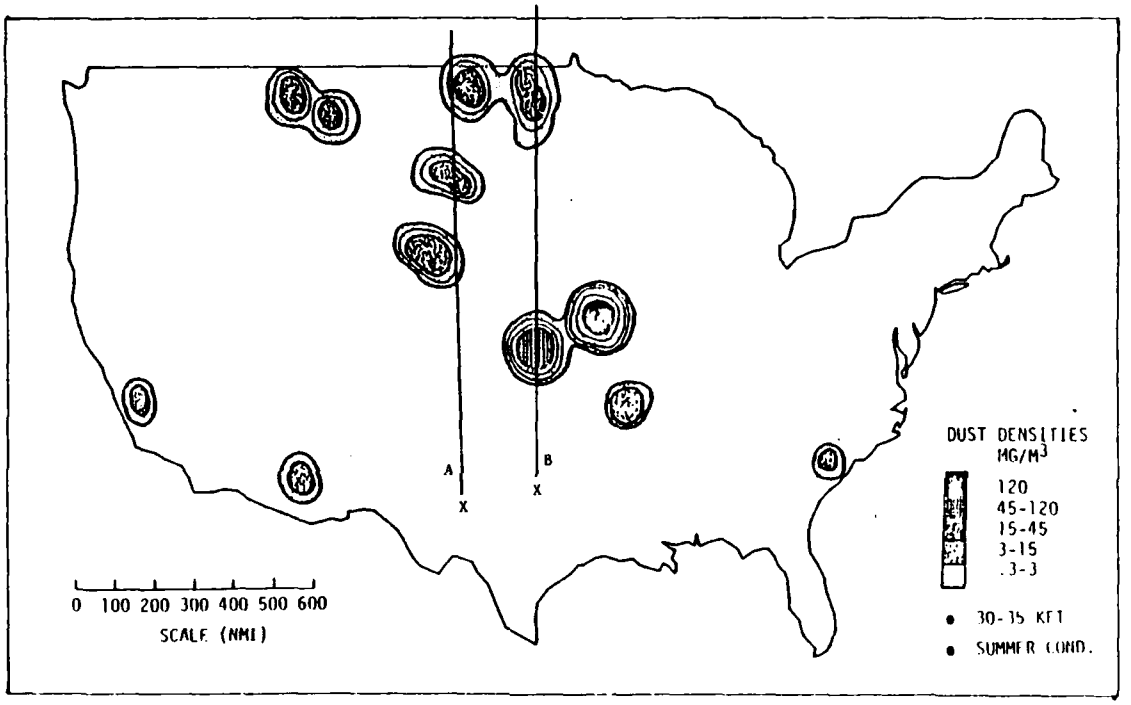

Figure 14. Dust cover for aircraft at 1 hour after laydown (Yoon, 1983).

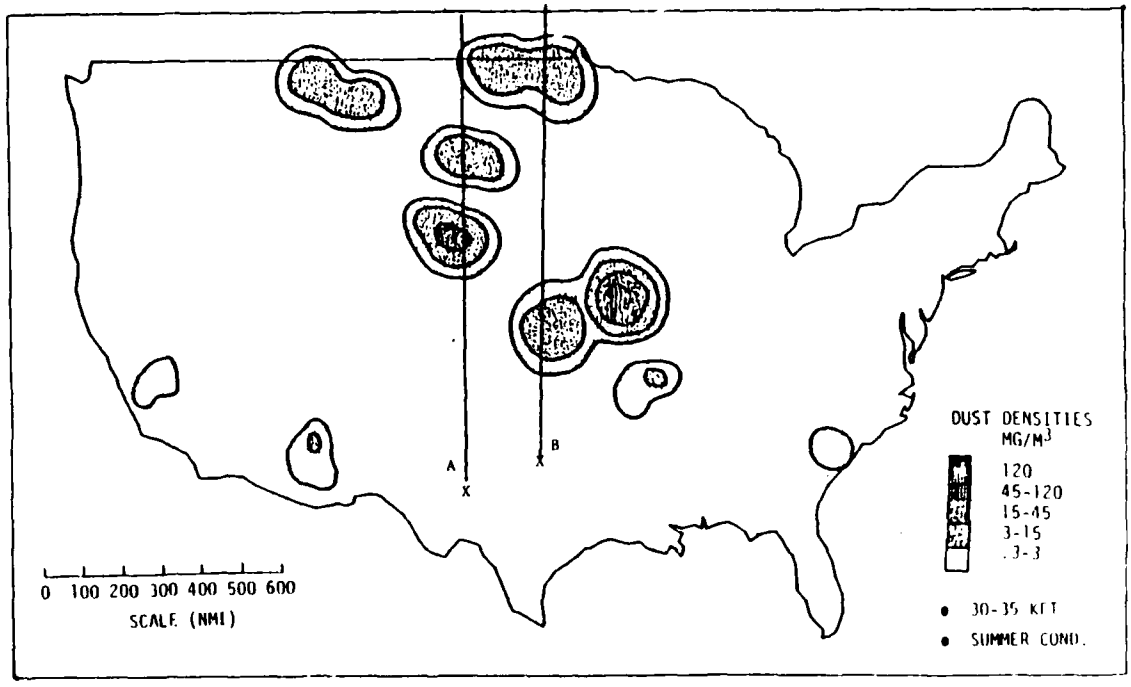

Figure 15. Dust cover for aircraft at 3 hours after laydown (Yoon, 1983).

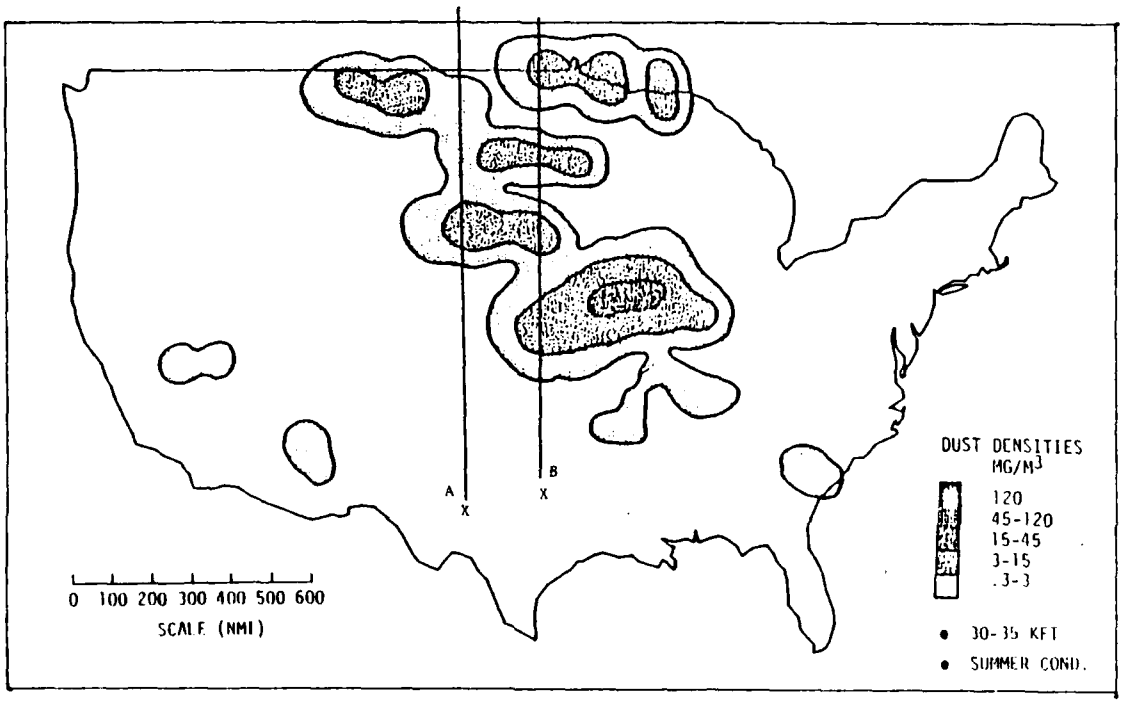

Figure 16. Dust cover for aircraft at 10 hours after laydown (Yoon, 1983).

laydown as indicated in Figure 17. For the restricted conditions which can be investigated at the present time, Equation (5) reduces to

$$MDP = \frac{1}{\rho_t} \sum_j U \cdot n^{(j)} \cdot L^{(j)} \tag{16}$$

Normal impacts are assumed so there is no angular dependence. The erosion rate is then simply a function of the particle size and impact velocity. The particle size is determined from Figure 17 for the values of time after laydown and therefore is assigned a fixed value. Correspondingly the mean erosion rate remains unchanged which would not be the case if the time interval for the dust distribution was reduced to 15 min. For lack of a flight plan the aircraft velocity is also held constant, so from Equation (5) $|\underline{v}^{(j)}| \Delta t^{(j)} = L^{(j)}$ the distance the aircraft travels through dust with concentration $n^{(j)}$. The density of the generic composite is assumed to be 1.65 g/cc.

The MDP for trajectories A and B can now be evaluated for the conditions stated above. The MDPs for a range of conditions are listed in Table 4 for trajectory A and in Table 5 for trajectory B. Referring to Tables 4 and 5, it is seen that the amount of material removed for both the short- and long-time distributions is on the order of 1 mm (40 mil). The MDP values can vary widely from this value due to the uncertainties in the erosion data as well as the dust distribution calculations. Also no effort was made to make worst case predictions. Flight through higher dust concentration zones would increase the removal rates several fold.

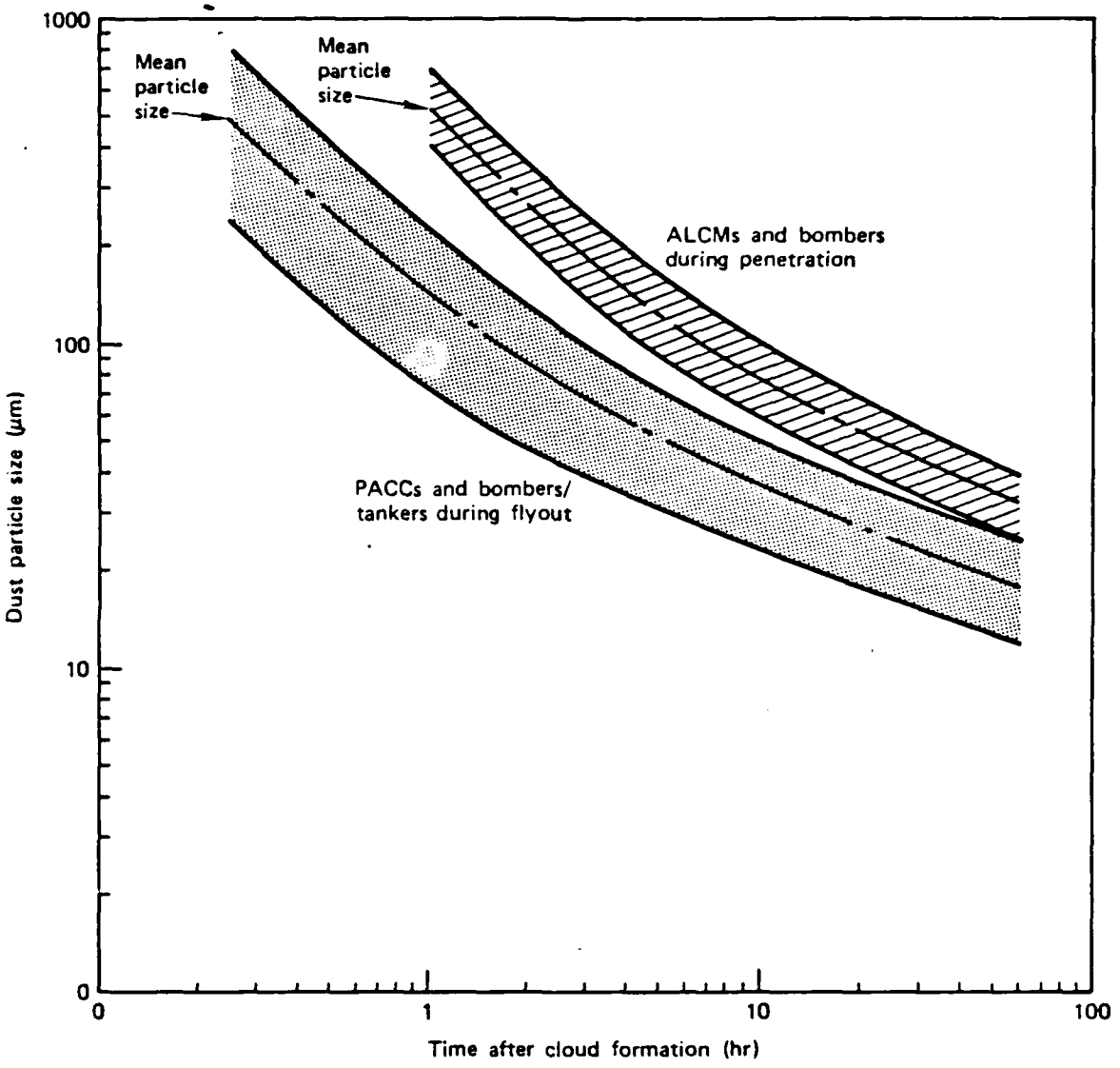

Figure 17. Particle size ranges as a function of cloud age (Yoon, 1983).

Table 4. Mean depth of penetration estimates for flight trajectory A.

Time (hr)	Particle Size (μm)	Dust Concentration (mg/m^3)	Distance (m)	Impact Velocity (ms^{-1})	Mass Loss Ratio (mg/g)	MDP (mm)
1	143	30	1.53×10^5			
		9	2.83			
		1.5	0.65	300	55-70	0.24-0.31
				342	75-95	.33- .42
				400	110-138	.48- .61
3	70	30	0.87×10^5			
		9	3.70			
		1.5	3.92	300	40-60	0.16-0.24
				342	53-84	.21- .33
				400	84-131	.33- .52
10	38	9	6.68×10^5			
		1.5	2.18	300	27-41	0.10-0.16
				342	36-58	.14- .22
				400	65-100	.25- .38

Table 5. Mean depth of penetration estimates for flight trajectory B.

Time (hr)	Particle Size (μm)	Dust Concentration (mg/m^3)	Distance (m)	Impact Velocity (ms^{-1})	Mass Loss Ratio (mg/g)	MDP (mm)
1	143	80	1.96×10^5			
		30	2.83			
		9	1.31			
		1.5	1.96	300	55-70	0.86-1.09
				342	75-95	1.18-1.49
				400	110-138	1.72-2.16
3	70	9	7.19×10^5			
		1.5	3.60	300	40-60	0.18-0.28
				342	53-84	.24- .38
				400	84-131	.38- .60
10	38	9	7.19×10^5			
		1.5	7.84	300	27-41	0.13-0.19
				342	36-58	.17- .27
				400	65-100	.30- .46

SECTION 5

DISCUSSION

The relevant erosion data, five experimental data points in Figure 13, for two different, ill-defined graphite-fiber reinforced composites has been used as the basis for constructing highly speculative relations between the erosion rates and the particle dimensions. This data is required since the mean particle dimensions in the dust environment predictions are a function of the time after cloud formation (Figure 17). The erosion rates recorded in Figure 13 can vary considerably from the stated values due to the high degree of uncertainty in the test procedure and the quality of the test specimens compared to current composite materials. However the information provided is indicative of the prevailing state-of-the-art for solid particle erosion of nonmetallic composites and coated materials for impact velocities in the vicinity of Mach 1. Figure 13 represents the best estimates that can be made without initiating additional testing to remove the prevailing data gap. The dust environment predictions also contain a high level of inherent uncertainty which could significantly influence the magnitude of the estimated material removal rates. In view of all of these factors and additional considerations which will be discussed shortly, it is evident the detrimental effects of the dusty environments which may be encountered by composite aircraft components cannot be ignored.

The 90° particle impact data used to make the MDP estimates in Tables 4 and 5 may not be the worse case condition. Based on the experimental erosion rates for various composite materials, it appears that the critical impact angle (the angle at which the maximum erosion rate occurs) is dependent on the type of composite material being evaluated. The critical impact angle can range from 30° to 90° (Figure 10). Maximum erosion rates are seen to occur at 45° (Figure 8) and 65° (Figure 9). Thus, until the erosion rates are measured for a specific composite construction, there is no assurance that non-normal

impingement angles will be beneficial in alleviating the severity of the amount of material removed.

The material removal evaluated in Tables 4 and 5 is for aircraft velocities in the vicinity of Mach 1; however if the flight velocity increases to Mach 2, the material removal is increased by a factor of 5.28 according to the power law relation for the erosion rates obtained from Behrendt's (1974) data. Extrapolation to the higher velocity assumes that no significant change occurs in the mode of material removal between these two velocities.

The erosion data for the graphite-reinforced polymers listed in Table 3 was used to provide the estimates of mass removal in Tables 4 and 5. If the erosion data for a material with the characteristics of fiberglass was used instead, the mass removal could conceivably increase by a factor of 2.5 for the normal impact condition. On the other hand, a more resilient matrix material than epoxy (the nylon composites in Table 3) could help to reduce the mass removal. The variation of more than an order of magnitude in the experimental erosion rates for different composite materials tends to reinforce the need for establishing reliable erosion data for a specific composite construction.

The possibility exists for aircraft which have been exposed to dust to subsequently encounter rain along their flight path. Although it may exist, no experimental data could be found for providing insights into the synergistic effects of the sequential imposition of a dust and rain environment on any material. The interaction between the erosion characteristics for each of these particle types could be quite strong and warrants consideration if the potential for damage is to be representative of a broad range of flight scenarios. While no directly applicable erosion data is available, conjectures can be made as to the extent of the material loss based on a knowledge of the erosion behavior of materials individually exposed to these two erosive environments. In particular, Adler (1973) evaluated the rain erosion behavior of the

graphite-reinforced epoxy material in Table 3 as well as its solid particle erosion characteristics. The rain erosion data is shown in Figure 18. The rain field is calibrated to 1.8 mm mean diameter water drops falling at the rate of 2.54 cm/hr.* It is seen that some time (the incubation period) is required before any rapid rate of material removal takes place. Finally a steady-state rate of removal is achieved. Using the information in Adler's report, the number of drops impacting the specimen and correspondingly the mass of water impacting the surface can be approximated. The steady-state erosion rate (for 1.8 mm diameter drops) was evaluated from Figure 18 and was found to be 52 mg/g compared to 19.1 mg/g for the solid particle environment. The same specimen geometry, a half cylinder, was used in the rain erosion tests also. If the region of the leading edge in which the drop impacts normal to the surface of the specimen was used in the above erosion rate evaluation instead of the projected area of the specimen, the erosion rates would be significantly higher (possibly by as much as a factor of four).

The general character of the damage is distinctly different in each case. The multiple solid particle impacts produce a relatively smooth eroded surface with each particle removing a small, localized volume; the water drops can penetrate the bulk of the specimen once cracks and pits are formed on the surface and remove relatively large volumes of material by a surface penetration and upheaval mechanism (Adler, 1979b).

Returning to the potential for enhanced damage in combined environments, it would seem that a surface preconditioned by solid particle impacts would provide numerous sites for the initiation of rain erosion damage. In other words, the long incubation period in Figure 18

---

*The rainfield in the AFML/Bell rotating arm facility was recalibrated and the plumbing system improved in 1978. Deviations in the previously stated and actual rainfield parameters were uncovered at that time, so the erosion rate could be changed simply due to the calibration difference.

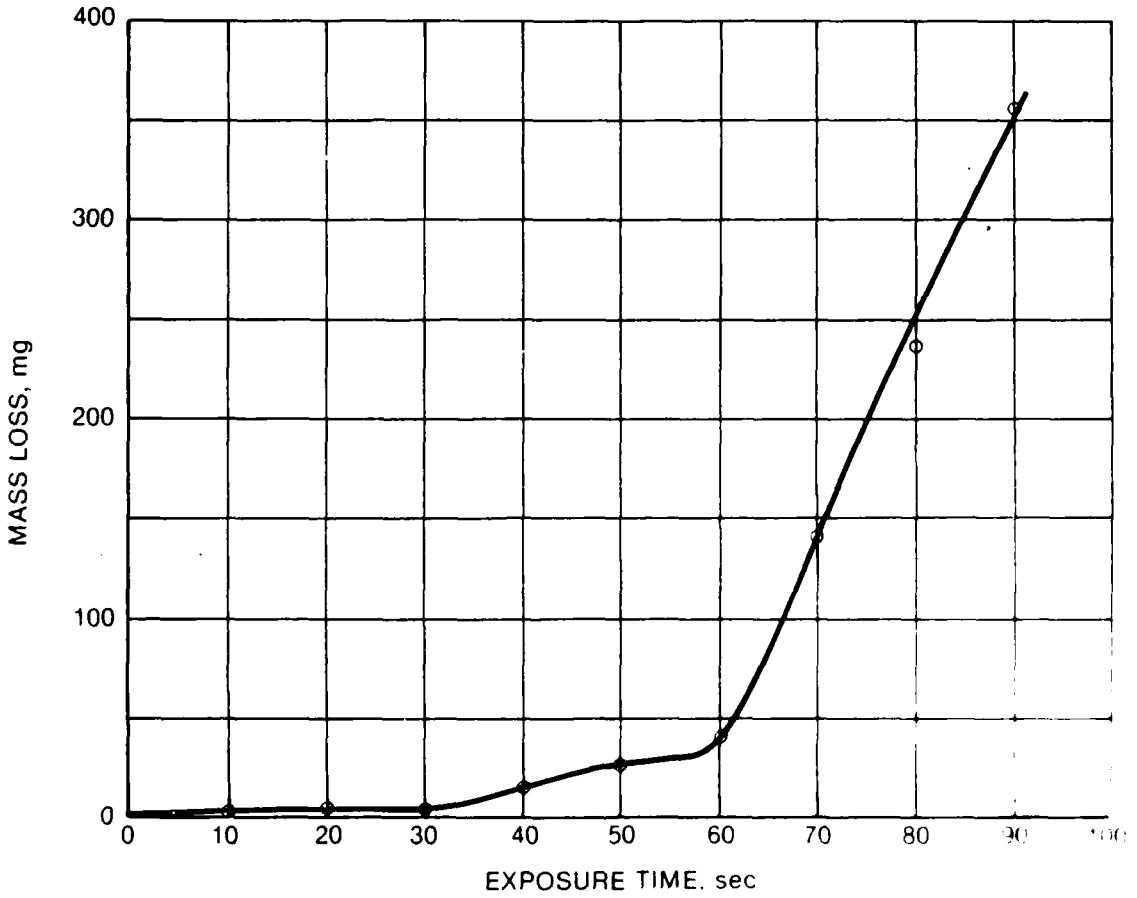

Figure 18. Mass loss for graphite-fiber reinforced epoxy specimens exposed to 10.29 1.8 mm water drop impacts/cm^2-sec. at 730 fps (222 ms^{-1}) (Adler, 1973).

(the duration of which is dependent on the impact velocity) would be by-passed and the steady-state erosion rates for the rain environment would be rapidly achieved. Also due to the pre-existing fractures, the effectiveness of the penetration and upheaval mechanism would be amplified for the rain drop collisions. The combined effect of exposure to a dust and then a rain environment should be much more severe than simply encountering a rain environment with a pristine material surface for a semi-brittle material. On the other hand, flight through rain followed by exposure to dust should produce only a slight increase in the solid particle erosion rates due to the localized nature of the solid particle impact damage. At this time these observations are conjectures and require experimental verification and quantification.

SECTION 6

EXISTING PARTICLE IMPACT TESTING CAPABILITY

The previous section provided an assessment of the prevailing data base for the particulate erosion of composite material constructions. The main conclusion from this survey is that there is essentially no data available for the types of materials which are of current interest. Another conclusion which is evident from this survey is that the number of existing facilities which can provide dust erosion data at impact velocities from 500 to 1500 fps is relatively small and the specimen dimensions are quite limited. The more positive result from this survey is the clear indication provided in Section 2 of how laboratory-scale test data can be utilized to provide estimates of the extent of the erosion damage on a wide range of materials for actual flight scenarios. The problem of how to obtain useful particulate erosion damage assessments will be addressed.

Particulate erosion tests are usually designed to satisfy one or more of the following three objectives: straightforward screening of materials exposed to a standard test condition, identification of damage mechanisms in order to improve the erosion resistance of a particular material, and the generation of data in support of a predictive modeling effort. The problem areas have mainly involved studying the effects of a single or relatively small number of particle impacts, such as, hypervelocity particle impacts on re-entry vehicle nosetips or water drop collisions on fragile infrared-transmitting materials or space shuttle tiles.

Motivated for the most part by the need for evaluating the relative rate of material removed due to solid particle or water drop impingement rather than in understanding the material removal process itself, a diversity of test configurations have been utilized to generate the screening assessments required. Erosion testing has

generally been undertaken to satisfy a very specific need for a particular application. Typically a test method is devised representative of the operational environment. A material selection procedure is pursued and then the testing is terminated. It is difficult to construct a coherent series of test results on this basis. On the other hand there have been a few programs which have been carried out to investigate the erosion process; these have been referred to fairly extensively in the erosion literature. Unfortunately, the available solid particle erosion test results have generally been reported with insufficient information pertaining to the test conditions to provide a valid comparison between the data obtained in one laboratory with that from another laboratory. This situation is complicated further by the fact that changes in the construction of the same test apparatus can significantly influence the delivery of particles to the target material as shown by Uuemois and Kleis (1975), Wolak, et al. (1977) and Maji and Sheldon (1979).

The primary reasons for the discrepancies in the correspondence between the erosive response of aircraft components based on erosion facility test results and their actual performance under operational conditions are:

- the lack of adequate characterization of the particle (sand or rain) interaction with the aerodynamic flow fields around the component during flight (recognizing that characterization of these particulate environments in general is a difficult problem),

- the lack of characterization and verification of the particle impact conditions within the erosion test facilities used to generate the erosion data,

- the lack of a procedure which indicates how the erosion test results relate to operational conditions.

The model described in Section 2 provides a general framework for relating erosion test results with the actual flight conditions and erosive environments in order to predict the material losses a structural component may experience. The model can be applied to material loss estimates for aircraft components. This model clearly indicates that once accurate erosion test data is obtained it can be used to evaluate a broad range of flight scenarios. This is a very significant result. This approach affords the opportunity to use a well-planned, laboratory-scale test program to generate a data base from which an unlimited number of flight scenarios and trade-off studies can be undertaken, compared with simulation tests which have a narrow range of application and have to be repeated as the flight conditions are changed. This is not to imply that the suggested approach is easy to implement, but once accomplished it has a considerably higher utility and cost-effectiveness than the alternatives.

The need for multiple solid particle collisions at impact velocities from 500 to 1500 fps limits the facilities which can achieve these particle impact requirements under reasonably controlled conditions. The types of facilities commonly used to obtain solid particle erosion data will be described and then the possibilities for satisfying the higher velocity requirements will be considered.

The most widely used test configuration for solid particle erosion is the sand blast apparatus. Although some version of this device has been used for laboratory-scale erosion evaluations for over seventy years, it has only been quite recent that the test parameters associated with particular types of equipment have been investigated. The sand blast equipment used for providing a multiple particle field ingests particulate matter into a flowing gas stream which subsequently impinges on a test piece through a small diameter tube: typically less than 12 mm (0.5 in). The impact velocity and angle of attack of the particles in the gas stream are governed in part by their size, shape, and density. The maximum particle impact velocities are generally less than 500 fps.

A facility of this type which operates at higher particle impact velocities was developed during the early 1970s at the Solar Turbines International, San Diego, California. In the Solar facility the dust is injected into a high-pressure air stream. The length of the delivery tube is on the order of 10 ft (3.05 m) so the particles have sufficient time in the air flow to achieve their terminal velocities. The particles exit the system through a 0.375 in (0.95 cm) nozzle. With this arrangement the eroded area is 0.11 in (0.71 cm) which may be marginal with respect to the construction of some of the composites which may be evaluated. The maximum air velocity is limited by the sonic velocity: 1120 ft/s (342 ms^{-1}). The maximum particle velocities depend on the mean size of the particles. The maximum particle velocity for a 10 μm particle is 935 ft/s (285 ms^{-1}); the impact velocity in this facility is greatly reduced for particles on the order of 100 μm. The particle impact conditions again fall short of the desired regime.

Another facility which provides higher-velocity dust erosion impacts (velocities up to 800 fps for 50 μm particles) was recently put in operation at PDA Engineering, Inc., in Santa Ana, California. The existing capability for this facility will be briefly described as it is known at the present time.

The particle impingement on the target is accomplished by translating the target across the particulate flow from one to four nozzles. The nozzle inside diameter is 0.19 in. and the spacing between the linear array of nozzles is about 0.25 in. The nozzle array can also be oscillated in an up and down motion which spreads the particles uniformly over a 0.5 in. high strip approximately 1.75 in. long. The test specimen is mounted to a 7 inch square plate that translates across the nozzles. The motions of this plate are computer controlled, so the traverse and speed at which the plate is moved can be regulated. Impact angles currently ranging from 20 to 90 degrees can be used. At impact angles less than 90 degrees the distance from the centerline of the

nozzle array to the impact location on the plate is maintained at a constant value once it is set.

The working area for uniform particle flows is about 6 inches square in order to account for end effects. PDA indicates that each location on the specimen receives the same particle distribution. The edges of the specimen are protected by placing a frame around the specimen. The specimen mounting conditions are flexible so the edge restraints can be designed to minimize the influence of the specimen boundaries on the rate of material removal. The maximum particulate exposure durations can range from 20 to 60 minutes depending on the particle size and the flow rate desired.

The particles are injected into the airflow from four fluidized beds which are charged with particles of a particular size. From one to four beds can be operating depending on the desired particle concentration. The particle concentration can also be changed by changing the flow rate in the fluidized bed. All four beds can contain the same particle sizes or the sizes can be different in each bed to provide a prescribed particle distribution. The particle velocity achieved for each particle dimension is dependent on the particle size, so the flow velocities have to be adjusted for each bed if a range of particle sizes is to impact the specimen at approximately the same velocity as would be the case for an aircraft flying into a dust cloud. The exactness of this condition is dependent upon the particle velocities within the dust cloud prior to colliding with the aircraft. The flow out of each nozzle is from a single fluidized bed, so mixing of particle sizes is accomplished by the translational motions of the test specimen past the nozzles. The particle velocities are determined using a xenon strobe and photographing the particles along a plane parallel to the flow direction.

Solid particles can also be injected into a flowing gas stream as in a wind tunnel. The specimen is then completely engulfed by the

particle-laden gas which offers the advantage of eliminating the transition region around the eroded spot on the test piece when the particles are propelled from a nozzle or tube as in the sand blast arrangement. A system of this type has been described by Grant and Tabakoff (1975) and Tabakoff and Wakeman (1979) at the University of Cincinnati. The maximum air velocity achievable in the dust erosion tunnel for ambient temperatures at the University of Cincinnati is 450 ft/s (140 ms^{-1}). Wind tunnels have been used in the past but the characterization of the dust environments in the tunnels was a problem in the early investigations. At the present time it does not appear that dust-laden airflows are incorporated into any existing transonic to low supersonic wind tunnel within the United States.

Rotating arm devices in which the specimen is mounted at the tip of a rotor blade and then passes through a stream of falling particles are also used for solid particle erosion evaluations (Kleis, 1969; Tilly and Sage, 1970; Adler, Morris, and Wahl, 1972). The rotating arm configuration has the advantage of having the specimen impact a graded particle distribution (such as specified by U.S. Military Specification, Mil-E-5007C, which includes particle sizes over the range from 0 to 1000 um at a uniform velocity. Such conditions are characteristic of high speed structural components in a dust field where the particles are traveling at considerably lower velocities. The rotating arm configurations also have potential for being operated at higher impact velocities compared with sand blast and wind tunnel test facilities, but the sample mass and dimensions are quite small and the sample configurations are also highly restricted. Bell Aerospace Textron rotating arm can operate at velocities of around 100 ft/s to about 3000 ft/s. However as Mach 1 is exceeded the sample dimensions are limited.

The variations which exist in solid particle erosion test apparatus, even for sand blast devices, make it difficult to discuss typical, or standard, test conditions. Generally the test results are strongly related to the test apparatus used. In addition the testing

procedures for solid particle erosion vary widely from laboratory to laboratory, so it is difficult to make an absolute comparison between the results obtained for one set of test conditions to another. Also, as more attention is paid to the test procedures and characterization of the impact conditions, additional factors which invluence the impacting particle/target interactions are being discovered (Tilly, 1969; Tilly and Sage, 1970; Uuemois and Kleis, 1975; Grant and Tabakoff, 1975; Wolak, et al., 1977; Young and Ruff, 1977; Tabakoff, Kotwal, and Hamed, 1979; Maji and Sheldon, 1979; Lapides and Levy, 1979). Therefore at the present time the test facility and the test procedure must be considered in conjunction with the test results.

Surveys of solid particle erosion testing facilities and procedures indicate there is a definite need for devising a facility to provide an accurate measure of the erosive response of materials and/or to provide detailed characterization of the actual impact parameters for existing facilities. This is not a simple undertaking due to the number of parameters which are associated with multiple collisions of irregular-shaped particles on a material surface whose general topography and properties are changing with the length of the exposure. The characterization process for a single particle type and material is in itself quite extensive. Many factors have to be evaluated to develop accurate measures of the mass of particles actually contacting the surface, their impact velocity and impingement angle, and the nature of the particles delivered to the surface compared with the initial properties and size of the particles (especially for soft particulates). Concentration effects are obviously important. Particle concentration can influence the extent of particle shielding at the surface (the accumulation of particles on the surface which prevents the incoming particles from making direct contact with the target's surface), particle rebound characteristics which change as a function of exposure time also affect the trajectories of the incoming particles, and the occurrence of particle embedding in the target's surface modifies the measured erosive response of the base material.

An overview of the evaluation of the system implications of aircraft flying through nuclear-generated dust environments will be described in the next section. The explicit erosion testing requirements will be outlined in conjunction with this overview.

SECTION 7

GENERAL EXPERIMENTAL REQUIREMENTS

The statement is often made that the erosion data obtained from laboratory-scale erosion facilities is not applicable to the conditions prevailing for actual flights through dusty environments. Contrary to this commonly-accepted observation, it is our opinion that if the laboratory data is used in the right way, very realistic predictions can be made of the erosive losses for a broad spectrum of aircraft flight scenarios. This approach offers the advantage of not having to carry out a significant number of costly flight tests even if it was possible to undertake full-scale testing in dusty environments. Since it is highly impractical to fly aircraft in dusty environments representative of nuclear-generated dust, the suggested laboratory-scale testing provides a viable solution. The accuracy of the erosive loss predictions is merely dependent on the level of effort devoted to the adjunct analyses required to transform the laboratory erosion data to the aircraft flight conditions. The statements made in Section 2 are reiterated, since it should be understood from the outset that once reliable, laboratory erosion data is obtained for the range of conditions which will be specified, this data remains valid for all flight scenarios and environmental conditions which may be considered.

The analyses and observations from Sections 2 and 6 provide the background for a meaningful approach for an assessment of the potential dust erosion damage to aircraft flying at high subsonic to low supersonic speeds. An overview of how such an assessment can be accomplished is outlined in Figures 19 and 20. The interrelationships in Figure 19 provide a clear perspective for the main features of the dust erosion assessment. The output from the analyses and experimental data generation will be a computational model for describing the extent of the material removal which may occur for an arbitrary flight plan.

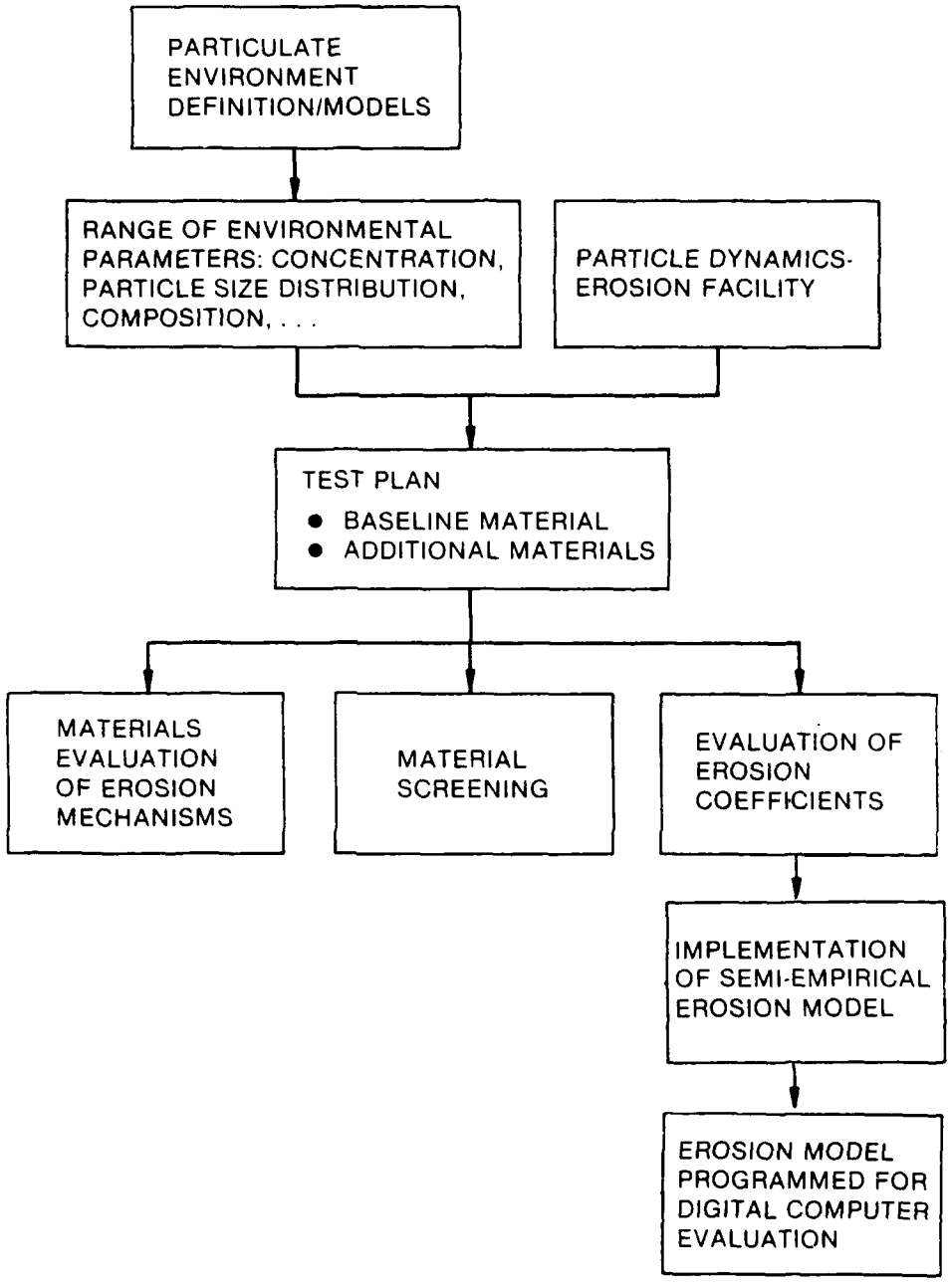

Figure 19. Assessment of erosion for aircraft component materials.

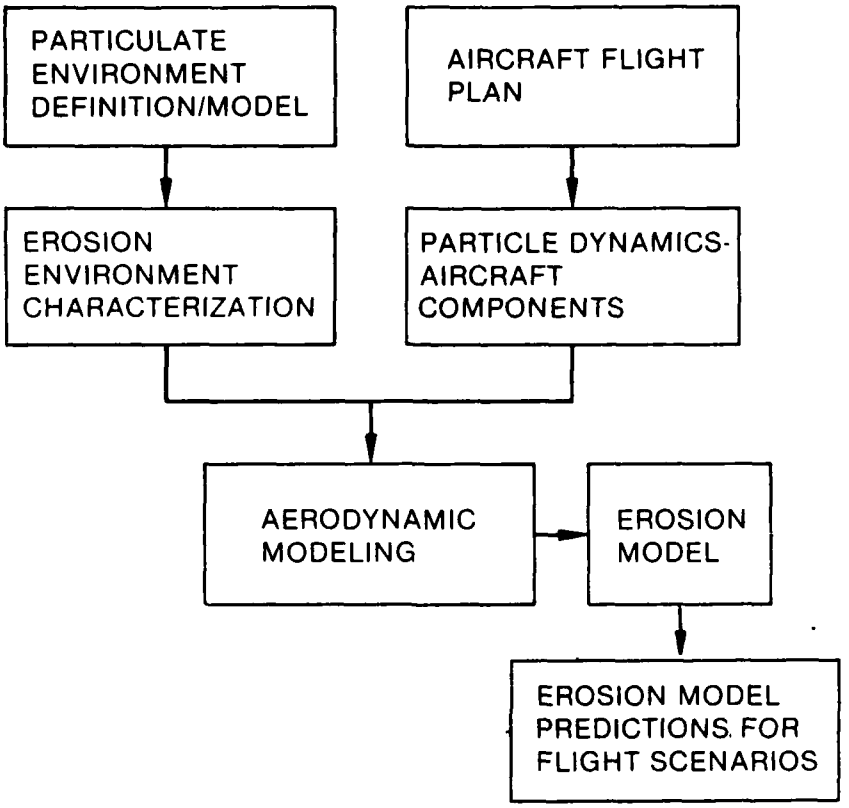

Figure 20. Prediction of dust erosion effects on aircraft components.

The resulting computational model may be used to examine a wide range of flight conditions.

The primary constituents of the computational model listed in Figure 19 will be described. It is important to note that estimates of the mass removal can be made using a minimal amount of information. As the inputs to the general approach are refined the uncertainties in the erosion predictions will correspondingly be reduced.

Either a superficial or detailed description of the erosive environment can be used to bracket the particulate impact conditions which will be significant. The initial survey of the particle impact parameters is used to limit the number of particle impact conditions which have to be considered. However subsequent modification of the dust environments will not alter the erosion test conditions. They should be selected to be broad enough to accommodate the anticipated dust environments. Since a very detailed and complete erosion test matrix can become overwhelming from the standpoint of the scope of the test program required, judgment has to be exercised as to the conditions which will provide a reasonable test plan as well as a reliable data base. With proper selection of the test conditions the data base can be expanded with extrapolations of the experimental results.

The motivation for elaborating the utility of the experimental erosion data base is that it is sometimes thought that the high level of uncertainties associated with specifying the nuclear-generated dust environments should be reduced before any effort be devoted to developing a much more representative and reliable erosion data base than exists at the present time. While significant discrepancies in the impact parameters derived from the lofted dust and debris models and the dispersion of this dust in the atmosphere will alter the predictions of aircraft erosion, an initially conservative estimate can be provided by assuming a worst-case condition. If the resulting levels of material

removal are not significant, the investigation of the erosive effects does not have to be pursued further. If the resulting predictions of material loss are marginal or unacceptable, further refinement of the dust environments to be encountered would be warranted. As the nuclear-generated dust models are refined, specification of the revised dust environments can be readily and easily incorporated into the erosion assessment. A much more important consideration for implementing the suggested approach is to provide reliable laboratory erosion data.

In order to obtain reliable erosion data, the particle impact conditions within the laboratory erosion facility and the particle impact conditions at the surface of the vulnerable aircraft components should be well-characterized. This aspect of utilizing the laboratory erosion data is usually neglected and leads to the general lack of correspondence between the laboratory results and the actual flight conditions. In the approach shown in Figures 19 and 20 it is very important that the aerodynamics of incoming particles impacting the test specimens in the erosion test facility and for the aircraft be defined. In the erosion facility this can be accomplished using diagnostic equipment to directly observe the particle impacts in addition to analytically defining their trajectories. For the aircraft the particle trajectories will more likely have to be specified from analytical or computational models. The difference in these particle impact conditions has been explicitly introduced in Equation (5). The level to which these particle impact conditions can be prescribed will determine the accuracy of the predictions which can be made by this approach. The general relations for incorporating the experimental data and for predicting the mass removal for actual flight scenarios involves the explicit evaluation of in Equations (5) and (12) in Section 2.

Since a complete description of the mass loss as a function of the particle type, size, impact angle, impact velocity, and particle

concentration for a single material involves hundreds of particle impact tests, discretion has to be exercised in the number of impact tests which are reasonable. If a number of materials are to be evaluated, a baseline material can be selected and fairly extensively characterized. The test program for these additional materials can be limited to the extent that is necessary to at least establish the trends (with respect to impact angle, particle size and impact velocity) which are adequate to define their particulate erosive behavior relative to the baseline material. A limited number of test conditions can be prescribed for the new materials of the same general type in the test matrix and these data points superposed on the more complete curves for the baseline material. If the same general trends appear as for the baseline material, a limited number of tests will be sufficient to compare each new material with the baseline. If anomalies are noted then more tests (a second interaction) will be required to describe the behavior of the new material.

In addition to obtaining quantitative measures of the material removal rates the test program also offers the advantage of providing specimens for materials characterization. Microscopic examination of the damage produced from the onset of material removal to accelerated rates of material removal provides significant information on how the erosion resistance of a particular material can be improved. Identification of the erosion mechanisms can be accomplished by removing specimens at various stages of the erosion process. These can then be used to construct a physical description of the microscopic mechanisms responsible for the onset and subsequent progression of damage.

In order to gain some appreciation for the magnitude of the erosion test program a representative test plan will be outlined. Suppose only one type of dust is considered, for example, crushed quartz. The silica can be sieved in accordance with the standard Tyler sieve openings beginning with 38 μm. Four size ranges for the particle

sizes are reasonable spanning the dimensions from 38 to 180 μm. Since the impact angle dependence of the material removal rates for the candidate composites is not known, the impact angles of 15, 25, 45, 60, and 90 degrees would have to be included for the baseline material at least. The evaluation of the impact velocity dependence of the material removal rates would require a minimum of three impact velocities. There are now sixty particle impact conditions specified for determining the erosion coefficients, U in Equation (5), for the baseline material. However the evaluation of the steady-state erosion rates requires a series of repetitive exposures for each particle impact condition in order to obtain the curve illustrated in Figure 1. Possibly eight to nine exposures are required in the erosion facility for this purpose. The specimen has to be accurately weighed after each exposure and correlated with the mass of particulates impacted during each successive exposure increment. Thus for the baseline material possibly 500 incremental exposures to the dust environment are necessary to fully evaluate the erosion coefficients. At least triplicate specimens exposed to the same particle impact conditions are required to provide adequate confidence in the resulting erosion coefficients. How expediently this could be accomplished depends on the configuration of the facility used for the dust erosion testing.

Once the erosion coefficients have been evaluated, the particle impact conditions have been properly characterized, and the erosion model has been programmed for digital computations predictions of the erosion of aircraft materials can be made. This is the scheme shown in Figure 19. The erosion model is then combined with a definition of the dust environment which can be used as input data for the model and evaluations of the aerodynamic flow fields over the aircraft component of interest as indicated in Figure 20. Predictions of the extent of the material removal from this component can then be provided.

Without the option of instrumenting an aircraft and flying through a well-characterized dust environment, a more feasible assessment of the accuracy of the erosion predictions for the aircraft component may be obtained with wind tunnel tests for at least a section of the component. The general plan for conducting the wind tunnel tests is illustrated in Figure 21. The erosion model would be evaluated for the conditions within the wind tunnel. The predictions from the model would then be compared with the post-test measurements of the material removal from the actual aircraft component after a sufficiently long exposure to the particle impact conditions within the wind tunnel.

While the effort described in this section is substantial, it provides a rational approach for evaluating the dust erosion effects which in the long run will be cost-effective and will apply to a wide range of flight conditions.

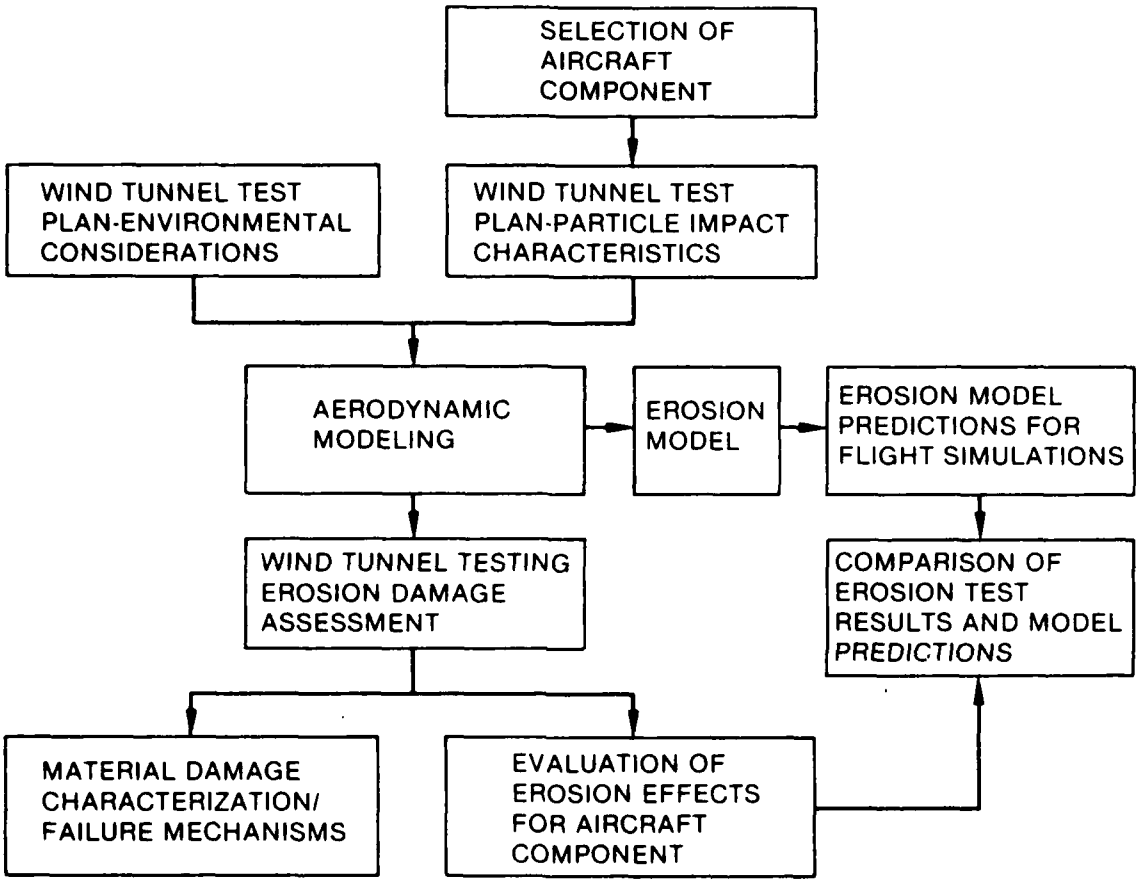

Figure 21. Comparison of erosion model predictions with simulated aircraft component flight conditions.

SECTION 8

CONCLUSIONS

The existing solid particle erosion data for non-metallic composite materials has been summarized and reviewed. This survey indicates that the erosion data for the particle sizes and impact velocities of interest is essentially not available. The limited number of erosion rates which are available have been used as the basis for a very preliminary estimate of the material removal which may be experienced by aircraft flying through dusty environments. This is certainly a highly speculative approach, but it represents the best estimates that can be made at the present time. The available data contains high levels of uncertainty, since it is for very ill-defined composite materials and the test procedures used may introduce significant errors.

An erosion model which clearly indicates the erosion and environmental parameters required and how they affect the material removal rates was used to predict the magnitude of the material removal which may occur for hypothetical flight scenarios. The indication from this initial effort is that the solid particle material removal rates for advanced composites can be significant.

This investigation, which represents the best material loss estimates that can be made currently, indicates that a properly directed experimental effort is required to improve the reliability of the damage assessment of composite aircraft components exposed to particulate environments.

SECTION 9

LIST OF REFERENCES

W. F. Adler (1973). Analytical Modeling of Liquid and Solid Particle Erosion, Air Force Materials Laboratory Report, AFML-TR-73-174 (September 1973).

W. F. Adler (1979a). "Particle Erosion of Electromagnetic Window Materials," Optical Engineering, 18, 610-619.

W. F. Adler (1979b). "The Mechanics of Liquid Impact," Treatise on Materials Science and Technology, vol. 16 Erosion (C. M. Preece, ed.), New York: Academic Press.

W. F. Adler (1979c). Assessment of the State of Knowledge Pertaining to Solid Particle Erosion, Final Report U.S. Army Research Office Contract No. DAAG29-77-C-0039, General Research Corp. Report No. CR-79-680 (30 June 1979).

W. F. Adler (1981). "Development of Design Data for Rain Impact Damage in Infrared Transmitting Materials," Proc. Soc. Photo Optical Instr. Engr., 297, Emerging Optical Materials.

W. F. Adler, W. Morris, Jr. and N. E. Wanl (1972). Supersonic Rain and Sand Erosion Research: Characterization and Development of Erosion Resistant Materials. Air Force Materials Laboratory Report AFML-TR-72-85 (May, 1972).

A. Behrendt (1974). "Sand Erosion of Dome and Window Materials," Proc. Fourth Int. Conf. on Rain Erosion and Assoc. Phenomena.

BMD Corporation (1984). Hardening of Manned and Unmanned Air Vehicles, unpublished.

J. E. Goodwin, W. Sage and G. P. Tilly (1969). "Study of Erosion by Solid Particles," Proc. Inst. Mech. Engrs., 184, 279-292.

G. Grant and W. Tabakoff (1975). "Erosion Prediction in Turbo-machinery Resulting from Environmental Solid Particles," J. Aircr., 12, 471-478.

M. E. Gulden (1979a). "Solid Particle Erosion of High-Technology Ceramics (Si_3N_4, Glass-Bonded Al_2O_3, and MgF_2)," Erosion: Prevention and Useful Applications, ASTM STP 664 (W. F. Adler, ed.). American Society for Testing and Materials, 101-122.

M. E. Gulden (1979b). Study of Erosion Mechanisms of Engineering Ceramics, Seventh Interim Technical Report, Effect of Number of Impacts on Erosion in the Elastic-Plastic Response Regime, Office of Naval Research Contract N00014-73-C-0401 (March, 1979).

I. Kleis (1969). "Probleme der Bestimmung des Strahlverschleisses bei Metallen," Wear, 13, 199-215.

L. Lapides and A. Levy (1979). "The Halo Effect in Jet Impingement Solid Particle Erosion Testing of Ductile Metals," in Erosion/Corrosion Newsletter (A. Levy) Pub-304, Lawrence Berkeley Laboratory, University of California (May 1979).

J. Maji and G. L. Sheldon (1979). "Mechanisms of Erosion of a Ductile Material by Solid Particles," Erosion: Prevention and Useful Applications, ASTM STP 664, (W. F. Adler, ed.). American Society for Testing and Materials, 136-147.

G. A. Sargent, P. K. Mehrotra, and H. Conrad (1979). "Multi-particle Erosion of Pyrex Glass," Erosion: Prevention and Useful Applications, ASTM STP 664 (W. F. Adler, ed.). American Society for Testing and Materials, 77-100.

G. L. Sheldon and I. Finnie (1966), "On the Ductile Behavior of Nominally Brittle Materials During Erosive Cutting," J. Eng. Ind. Nov. 1966, 387-392.

W. Tabakoff, R. Kotwal, and A. Hamed (1979). "Erosion Study of Different Materials Affected by Coal Ash Particle," Wear, 52, 161-173.

W. Tabakoff and T. Wakeman (1979). "Test Facility for Material Erosion at High Temperature," Erosion: Prevention and Useful Applications, ASTM STP 664 (W. F. Adler, ed.). American Society for Testing and Materials, 123-135.

G. P. Tilly (1969). "Erosion Caused by Airborne Particles," Wear, 14, 63-79.

G. P. Tilly and W. Sage (1970). "The Interaction of Particle and Material Behaviour in Erosion Processes," Wear, 16, 447-465.

H. Uumois and I. Kleis (1975). "A Critical Analysis of Erosion Problems Which Have Been Little Studied," Wear, 31, 359-371.

J. H. Williams, Jr. and E. K. Lau (1974). "Solid Particle Erosion of Graphite-Epoxy Composites," Wear, 29, 219-230.

J. Wolak, P. Worm, I. Patterson and J. Bodoin (1977). "Parameters Affecting the Velocity of Particles in an Abrasive Jet," J. Eng. Mat. Tech., 99, 147-152.

B. Yoon (1983). Nuclear Dust Cloud Characterization. Presented at DNA Aircraft Survivability/Vulnerability Meeting, 8 February 1983.

J. P. Young and A. W. Ruff (1977). "Particle Erosion Measurements on Metals," J. Eng. Mat. Tech., 99, 121-125.

J. Zahavi and G. F. Schmitt, Jr. (1981a). "Solid Particle Erosion of Reinforced Composite Materials," Wear, 71, 179-190.

J. Zahavi and G. F. Schmitt, Jr. (1981b). "Solid Particle Erosion of Polymeric Coatings," Wear, 71, 191-210.

DISTRIBUTION LIST

DEPARTMENT OF DEFENSE

ASST TO THE SECY OF DEFENSE ATOMIC ENERGY
ATTN: EXECUTIVE ASSISTANT

DEFENSE INTELLIGENCE AGENCY
ATTN: DB-6E V FRATZKE
ATTN: RTS-2B

DEFENSE NUCLEAR AGENCY
ATTN: SPAS
4 CYS ATTN: STTI-CA

DEFENSE TECHNICAL INFORMATION CENTER
12 CYS ATTN: DD

FIELD COMMAND DEFENSE NUCLEAR AGENCY
ATTN: FCTT W SUMMA
ATTN: FCTXE

FIELD COMMAND DNA DET 2
LAWRENCE LIVERMORE NATIONAL LAB
ATTN: FC-1

JOINT STRAT TGT PLANNING STAFF
ATTN: JLK (ATTN: DNA REP)

UNDER SECY OF DEF FOR RSCH & ENGRG
ATTN: DIR CRUISE MISSILE SYS
ATTN: STRAT & SPACE SYS (OS)
ATTN: STRAT & THTR NUC FORCES

DEPARTMENT OF THE ARMY

AVIATION APPLIED TECHNOLOGY DIRECTORATE
ATTN: DAVDL-ATL-ATP H MORROW

HARRY DIAMOND LABORATORIES
ATTN: SLCHD-NW-P J GWALTNEY 20240

U S ARMY AVIATION SYSTEMS CMD
ATTN: AMSAV-ES LTC DEVAUGHAN

U S ARMY BALLISTIC RESEARCH LAB
ATTN: S POLYAK
ATTN: SLCBR-TB-B R RALEY

U S ARMY NUCLEAR & CHEMICAL AGENCY
ATTN: LIBRARY
ATTN: MONA-NU MR LONG

DEPARTMENT OF THE NAVY

MARINE HELICOPTER SQUADRON ONE
ATTN: HMX-1/PLANS MAJ P HALTON

NAVAL AIR SYSTEMS COMMAND
ATTN: AIR 5164G
ATTN: PM-23

NAVAL AIR TEST CENTER
ATTN: SATD LCDR KOENIG

NAVAL RESEARCH LABORATORY
ATTN: CODE 2627 TECH LIB
ATTN: CODE 6006 D FORESTER

NAVAL WEAPONS CENTER
ATTN: CODE 3383 J MORROW

NAVAL WEAPONS EVALUATION FACILITY
ATTN: CLASSIFIED LIBRARY
ATTN: CODE 50 R FRIEDBERG

OFC OF THE DEPUTY CHIEF OF NAVAL OPS
ATTN: OP 654 STRAT EVAL & ANAL BR

STRATEGIC SYSTEMS PROGRAM OFFICE (PM-1)
ATTN: SP-272

DEPARTMENT OF THE AIR FORCE

AERONAUTICAL SYSTEMS DIVISION, AFSC
ATTN: ASD/B1ES E PRICE
ATTN: ASD/ENSS
ATTN: ASD/ENSSS H GRIFFIS

AIR FORCE CTR FOR STUDIES & ANALYSIS
2 CYS ATTN: AFCSA/SAMI R GRIFFIN
ATTN: AFCSA/SASB
ATTN: AFCSA/SASM MAJ TOM HOPKINS

AIR FORCE SYSTEMS COMMAND
ATTN: DLWM
ATTN: SDNI
ATTN: XRT

AIR FORCE WEAPONS LABORATORY, AFSC
ATTN: NTA A SHARP
ATTN: NTATE E FRANKLIN
ATTN: NTN (NGCS)
ATTN: SUL

AIR FORCE WRIGHT AERONAUTICAL LAB
ATTN: POTX M STIBICH

AIR FORCE WRIGHT AERONAUTICAL LAB
ATTN: GLXRM R DENISON

AIR FORCE WRIGHT AERONAUTICAL LAB
2 CYS ATTN: AFWAL MLBT W ANSPACH

DEPARTMENT OF THE AIR FORCE (CONTINUED)

AIR FORCE WRIGHT AERONAUTICAL LAB
ATTN: FIBAC J ROSELIUS
ATTN: FIBEB C SCHMIDT

AIR UNIVERSITY LIBRARY
ATTN: AUL-LSE

DEPUTY CHIEF OF STAFF/AF-RDQI
ATTN: AF/RDQI

DEPUTY CHIEF OF STAFF/AF/RD-L
ATTN: RD L

STRATEGIC AIR COMMAND/NRI-STINFO
ATTN: NRI/STINFO

STRATEGIC AIR COMMAND/XOBB
ATTN: XOBB
ATTN: XOKF MAJ A PHILPOTTS

STRATEGIC AIR COMMAND/XPF
ATTN: XPF

STRATEGIC AIR COMMAND/XPFS
ATTN: XPFS

DEPARTMENT OF ENERGY

SANDIA NATIONAL LABORATORIES
ATTN: TECH LIB 3141 RPTS RCVG CLRK

OTHER GOVERNMENT

CENTRAL INTELLIGENCE AGENCY
ATTN: OSWR/NED

U S ARMS CONTROL & DISARMAMENT AGCY
ATTN: H COOPER

DEPARTMENT OF DEFENSE CONTRACTORS

BOEING CO
ATTN: A DACOSTA

BOEING MILITARY AIRPLANE CO
ATTN: D SAWDY

CALSPAN CORP
ATTN: C PADOVA
ATTN: M DUNN

CARPENTER RESEARCH CORP
ATTN: H J CARPENTER

DAMASKOS, INC
ATTN: N DAMASKOS

DAYTON, UNIVERSITY OF
ATTN: B WILT

GENERAL RESEARCH CORP
ATTN: D MIHORA
ATTN: R CRAWFORD
6 CYS ATTN: W ADLER

IRT CORP
ATTN: D WOODALL

KAMAN SCIENCES CORP
ATTN: D COYNE
ATTN: L MENTE
ATTN: R RUETENIK
ATTN: W LEE

KAMAN SCIENCES CORP
ATTN: E CONRAD

KAMAN TEMPO
ATTN: DASIAC

KAMAN TEMPO
ATTN: DASIAC

LOCKHEED CORPORATION
ATTN: A SCHUETZ
ATTN: B OSBORNE

LOCKHEED-GEORGIA COMPANY
ATTN: A BONDERUD
ATTN: R KELLY
ATTN: T HODGSON

MCDONNELL DOUGLAS CORP
ATTN: H SAMS
ATTN: L KOCH
ATTN: R J PANDORF

MCDONNELL DOUGLAS CORP
ATTN: J TRACY
ATTN: L COHEN

MCDONNELL DOUGLAS CORP
ATTN: J GAIDULIS
ATTN: J MCGREW
ATTN: M POTTER

NORTHROP CORP
ATTN: B AGARWAL
ATTN: G KENDALL

PACIFIC-SIERRA RESEARCH CORP
ATTN: H BRODE, CHAIRMAN SAGE

R & D ASSOCIATES
ATTN: A KUHL
ATTN: F A FIELD
ATTN: P RAUSCH

RAND CORP
ATTN: P DAVIS

DEPT OF DEFENSE CONTRACTORS (CONTINUED)

RAND CORP
ATTN: B BENNETT

ROCKWELL INTERNATIONAL CORP
ATTN: A MUSICMAN
ATTN: P MASON
ATTN: S MELLINS

SCIENCE APPLICATIONS INTL CORP
ATTN: J COCKAYNE

SCIENCE APPLICATIONS INTL CORP
ATTN: A MARTELLUCCI

SOUTHERN RESEARCH INSTITUTE
ATTN: C PEARS
ATTN: S CAUSEY

TOYON RESEARCH CORP
ATTN: B GRAGG
ATTN: J CUNNINGHAM

END

1-87

DTIC